



GENERAL ATOMIC

E-117-833

THE U-ZrH_x ALLOY: ITS PROPERTIES
AND USE IN TRIGA FUEL

by
M. T. Simnad

GA Project No. 4314

February 1980

820428

8204280403

ABSTRACT

The uranium-zirconium-hydride (U-ZrH_x) fuel is an integral fuel-moderator system. Development, use, and marketing of the U-ZrH_x fuel technology has been underway at General Atomic since 1957. During this period over 6000 fuel elements have been fabricated for the TRIGA reactors. Over 25,000 pulses have been performed with the TRIGA fuel elements at General Atomic. The TRIGA fuel was developed around the concept of inherent safety.

The development and the characteristics of the TRIGA fuels are described in this paper. The fabrication techniques have been developed to the point where the production of fuel bodies containing controlled amounts of hydrogen and burnable poison (erbium) has been carried out in sizes from 0.5 to 1.5 in. in diameter. Instrumented fuel elements have been designed to determine the temperatures in the fuels and claddings and to record the gas pressures in the fuel elements, under both steady-state and pulsed operations. The metallurgical, physical, mechanical, and corrosion properties of the fuel are presented, along with empirical correlations relating irradiation behavior and fission product retention to temperature, composition, burnup, and neutron flux and fluence.

CONTENTS

ABSTRACT	i
1. INTRODUCTION	1-1
2. PROPERTIES OF HYDRIDE FUELS	2-1
2.1. Physical Properties	2-1
2.2. Hydrogen Density	2-1
2.3. Phase Systems	2-5
2.4. Dissociation Pressures	2-11
2.5. Hydrogen Migration	2-16
2.6. Hydrogen Retention	2-19
2.7. Density	2-19
2.8. Thermal Conductivity	2-24
2.9. Heat Capacity	2-25
2.10. Thermal Expansion	2-26
2.11. Mechanical Properties	2-31
2.12. Corrosion Properties	2-34
2.13. Irradiation Effects	2-39
3. PULSE HEATING	3-1
Erbium Additions	3-6
4. LIMITING DESIGN BASIS PARAMETER AND VALUES	4-1
5. FISSION PRODUCT RETENTION	5-1
6. THERMAL CYCLING TESTS	6-1
7. ACKNOWLEDGMENTS	7-1
8. REFERENCES	8-1
APPENDIX	

FIGURES

1-1.	Typical TRIGA fuel element	1-2
2-1.	Plateau pressures of the monohydrides and dihydrides of various metals	2-2
2-2.	One-atmosphere isobars in various metal hydrogen systems . . .	2-3
2-3.	Hydrogen density (N_H) versus H/Zr ratio for zirconium hydride at room temperature	2-4
2-4.	Zirconium hydride phase diagram, showing boundary determination	2-6
2-5.	Zirconium hydride phase diagram, enlargement of area under study	2-7
2-6.	Zirconium hydride phase diagram	2-8
2-7.	Zirconium-hydrogen phase relationships	2-9
2-8.	Dissociation pressure isochores of zirconium hydride (expressed as H/Zr atom ratios)	2-12
2-9.	Equilibrium hydrogen pressure over $ZrH_{1.65}$ versus temperature	2-13
2-10.	Hydrogen loss rate through 10-mil-thick stainless steel moderator can	2-20
2-11.	Permeability of various metals to hydrogen (1-mm-thick metal)	2-21
2-12.	Density of delta and epsilon phases of zirconium hydride as determined by x-ray diffraction	2-22
2-13.	Density diagram	2-23
2-14.	Specific heat curves for delta and epsilon phases	2-27
2-15.	Zirconium hydride phase diagram with isobars and isometrics	2-30
2-16.	Bow of a UZrH rod resulting from an asymmetric thermal gradient	2-30
2-17.	Creep properties of zirconium hydride; comparison of β with δ and $\delta + \epsilon$ phase material	2-32
2-18.	Ultimate tensile strength and percent elongation of zirconium hydride at 600°C	2-33
2-19.	Fuel sample 9 after quench from 1200°C	2-38
2-20.	Zirconium hydride fuel swelling	2-47
2-21.	Radial fuel growth vs time (based on fuel cladding ΔT)	2-48
2-22.	Volume increase vs burnup for the 1300°F subcapsules (based on fuel-cladding ΔT)	2-48

FIGURES (continued)

2-23.	Fuel growth vs burnup with NAA-53, NAA-115-1, and empirical correlations	2-49
2-24.	Fuel growth vs burnup with NAA-53 and NAA-75 data	2-49
4-1.	Strength of type 304 stainless steel as a function of temperature	4-3
4-2.	Fuel element internal pressure versus time after a step increase in maximum fuel temperature	4-5
5-1.	Fractional release of gaseous fission products from TRIGA fuel showing theoretical maximum, and experimental values above 400°C corrected to infinite irradiation.	5-3
5-2.	Photographs of uranium x-ray distribution maps in TRIGA fuel specimens. (A) 8.5 w/o-20% enriched, (B) 30 w/o, (C) 45 w/o and (D) 45 w/o-20% enriched	5-8

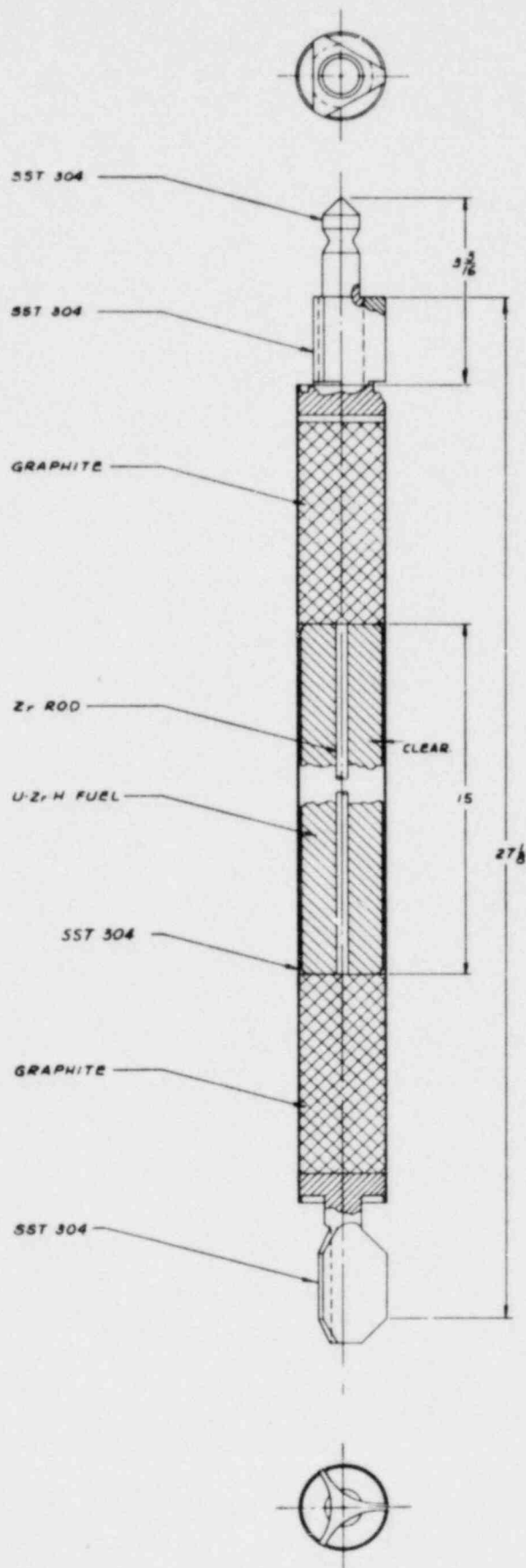
TABLES

2-1.	Thermal expansion	2-28
2-2.	Characteristics of 45U-53Zr-1Er-1H samples before and after quench tests	2-37
2-3.	Selected data from capsule irradiation tests	2-46
5-1.	Summary of metallographic and microprobe examination	5-7
6-1.	Results of thermal cycling tests	6-2

1. INTRODUCTION

The development and use of U-ZrH_x fuels for the TRIGA reactor has been under way at General Atomic since 1957 (Refs. 1 through 10). Over 6000 fuel elements (Fig. 1-1) of 7 distinct types have been fabricated for the 60 TRIGA research reactors which are under construction or have been placed in operation. The earliest of these are now passing 20 years of operation. The first TRIGA reactor to be exported was for the U.S. exhibit at the Second Geneva Conference on the Peaceful Uses of Atomic Energy in 1958 (see Appendix).

The standard TRIGA fuel contains 8.5 to 12 wt % uranium (20% enriched) as a fine metallic dispersion in a zirconium hydride matrix. The H/Zr ratio is nominally 1.6 (in the face-centered cubic delta phase). The equilibrium hydrogen dissociation pressure is governed by the composition and temperature. For $\text{ZrH}_{1.6}$ the equilibrium hydrogen pressure is one atmosphere at about 760°C. The single-phase, high-hydride composition eliminates the problems of density changes associated with phase changes and with thermal diffusion of the hydrogen. Highly enriched versions of TRIGA fuels (discontinued in 1979) contained up to about 3.0% erbium as a burnable poison to increase the core lifetime and contribute to the prompt negative temperature coefficient in the higher power (1 to 14 MW) TRIGA reactors (Refs. 8, 9). (Cores with steady-state power levels above 3 MW are not pulsing cores.) The calculated core lifetime with FLIP fuel in the 2-MW TRIGA is approximately 9 MW-yr. Over 25,000 pulses have been performed with the TRIGA fuel elements at General Atomic, with fuel temperatures reaching peaks of about 1150°C.



LC45755

EL-1249

Fig. 1-1. Typical TRIGA fuel element

TRIGA fuel was developed around the concept of inherent safety. A core composition was sought which had a large prompt negative temperature coefficient of reactivity such that if all the available excess reactivity were suddenly inserted into the core, the resulting fuel temperature would automatically cause the power excursion to terminate before any core damage resulted. Experiments then in progress demonstrated that zirconium hydride possesses a basic mechanism to produce the desired characteristic. Additional advantages were that ZrH has a good heat capacity, results in relatively small core sizes and high flux values due to the high hydrogen content, and could be used effectively in a rugged fuel element size.

In early 1976, General Atomic undertook the development of fuels containing up to 45 wt % uranium in order to allow the use of low enriched uranium (LEU) (under 20% enrichment) to replace the highly enriched fuels while maintaining long core life. These fuels were fabricated successfully, with the required hydrogen content and erbium loading. The structural features of the hydrided LEU fuel were similar to those of the well-proven 8.5 and 12 wt % fuels, as shown by metallographic, electron microprobe analysis, and x-ray diffraction examination. The uniform distribution of the uranium on a macroscale and the distribution of the various phases were as expected from the experience with the standard fuel. The high-U LEU fuels were subjected to thermal cycling, pulsing tests to 725°C, and water quench tests from 1200°C, which they survived successfully. The physical and thermal stability properties of the LEU fuels are acceptable. Very low release fractions of fission products were measured at normal operating temperatures, with the temperature dependent functions describing the fission product release rate for standard TRIGA fuel still remaining applicable to the TRIGA-LEU fuel. Previous work on U-ZrH_x fuels during the SNAP reactor program had developed the technology up to 20 wt % uranium and found no indication of this being a limit. Burnup of U-235 reached values of about 80% in SNAP program

tests. (Other nuclear applications of metal hydrides are described in Refs. 11 through 18.) Ongoing in-core tests at General Atomic with 20 and 45 wt % fuel, started in April 1978. These tests have been an unqualified success during pulsing and steady-state operation including over 2000 thermal cycles where the reactor has gone from shutdown to powers of 1 to 1.5 MW. An irradiation test of a standard 16-rod cluster configuration is being tested in the 30 MW ORR Reactor at Oak Ridge.

The high-U LEU fuel was also subjected to water-quench safety tests by quenching from temperatures up to 1200°C. The results showed that this fuel also survives the quench tests with a benign response, with only minor cracking, volume shrinkage, loss of hydrogen, and surface oxidation.

2. PROPERTIES OF HYDRIDE FUELS

2.1. PHYSICAL PROPERTIES

The hydrogen atom density in hydrides is generally expressed in terms of N_H , the number of hydrogen atoms per cubic centimeter of hydride $\times 10^{-22}$. This is calculated from the hydrogen-to-metal atom ratio H/M , the density of the hydride ρ , and the molecular weight W by the expression $N_H = [(H/M)(\rho)(60.23)]/W$.

The plateau pressures of the monohydrides and dihydrides of various metals are shown in Fig. 2-1, which demonstrates the wide range in the thermal stabilities of the hydrides. The one-atmosphere isobars in various relatively stable metal hydrides are shown in Fig. 2-2. Isobars at higher pressures will be at larger N_H and higher temperatures. The isobars provide a comparative measure of stabilities of the hydrides as a function of temperature and is useful for comparing the N_H parameter before consideration of other important criteria such as neutron capture cross section, physical and mechanical properties, radiation stability, cost, and availability.

Zirconium hydride has a very high N_H and good thermal stability. Its range of compositions extends up to ZrH_2 . At a composition having an N_H equivalent to that of water (6.7), zirconium hydride can be used at temperatures as high as 750°C under steady-state and 1200°C under short transient pulse operation.

2.2. HYDROGEN DENSITY

The hydrogen density N_H versus the H/Zr ratio for zirconium is given in Fig. 2-3 (Ref. 18).

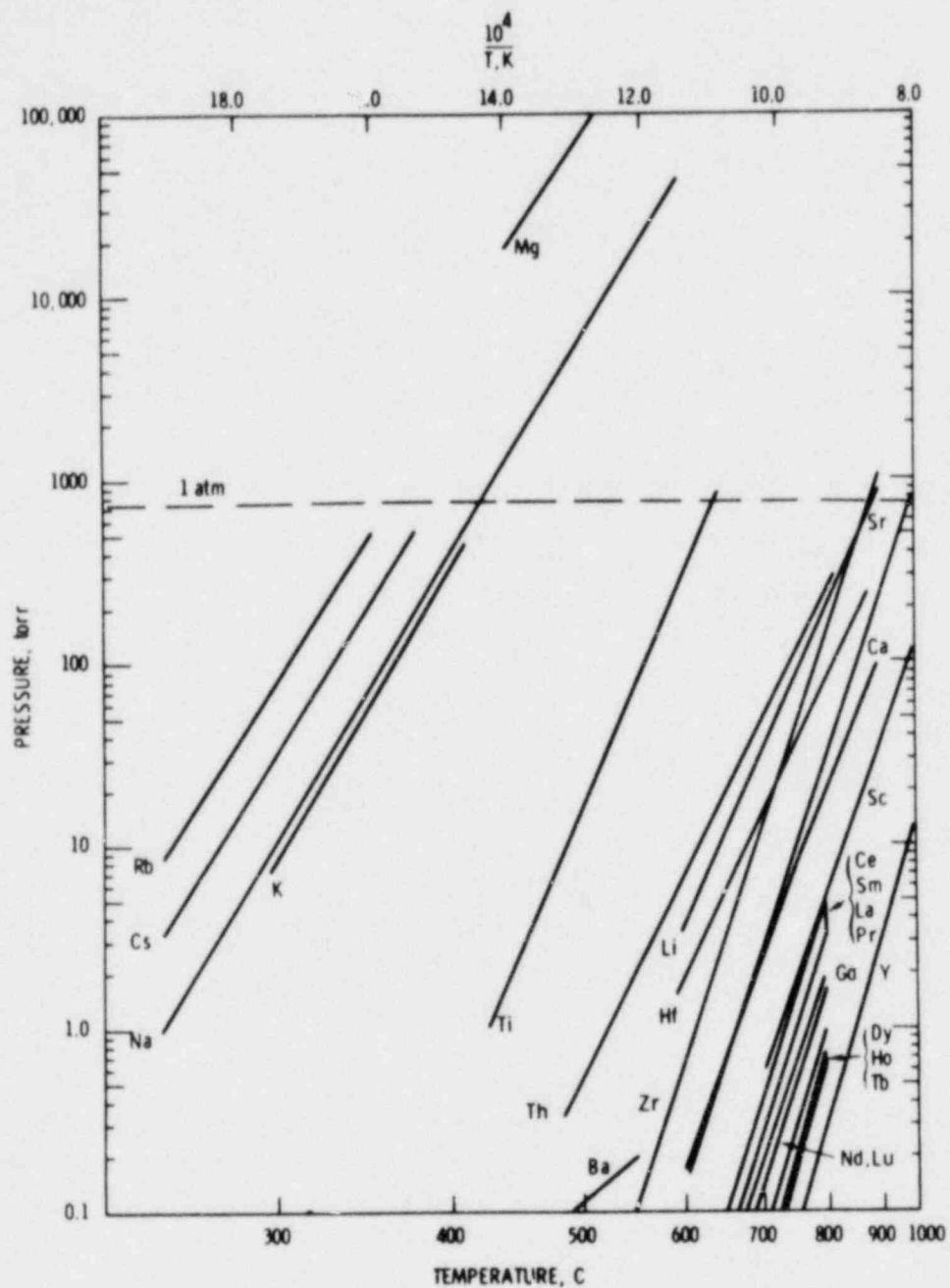


Fig. 2-1. Plateau pressures of the monohydrides and dihydrides of various metals (from Ref. 17)

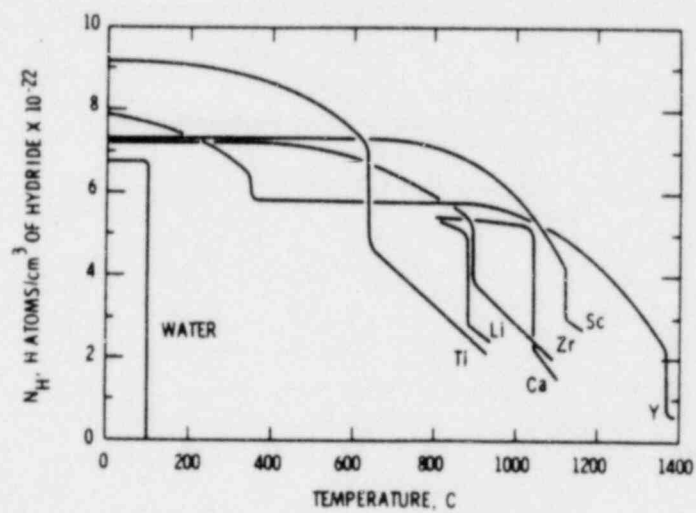


Fig. 2-2. One-atmosphere isobars in various metal hydrogen systems (from Ref. 17)

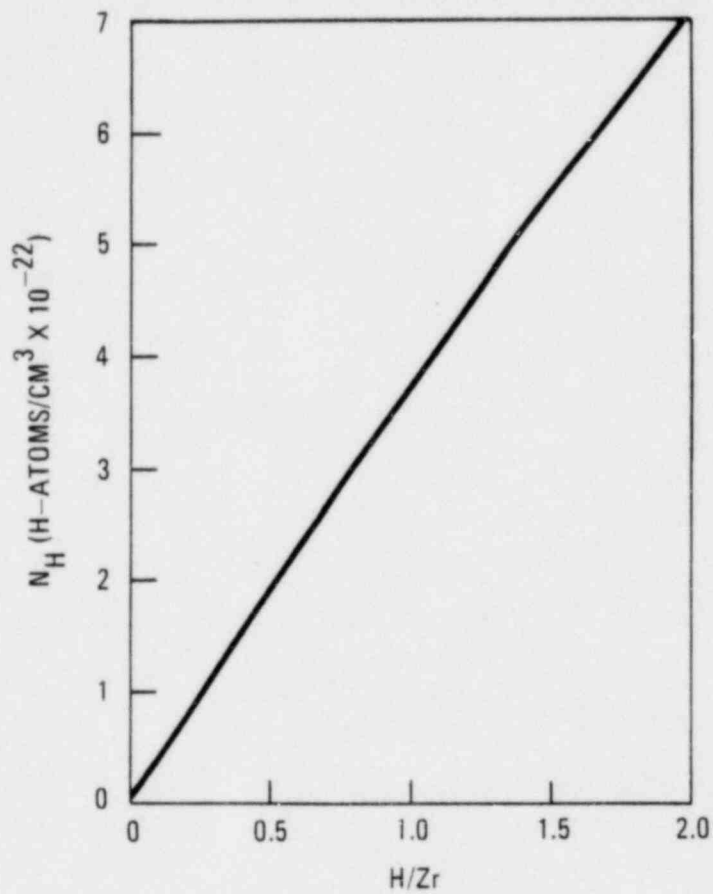


Fig. 2-3. Hydrogen density (N_H) versus H/Zr ratio for zirconium hydride at room temperature (from Ref. 18)

2.3. PHASE SYSTEMS

The ZrH system is essentially a simple eutectoid (Refs. 19, 20) containing at least four separate hydride phases in addition to the zirconium and allotropes (Figs. 2-4 through 2-7). The hydride phases consist of the following:

1. Alpha phase: a low-temperature terminal solid solution of hydrogen in the hexagonal, close-packed, alpha zirconium lattice.
2. Beta phase: a solid solution of hydrogen dissolved in the high-temperature, body-centered cubic zirconium phase.
3. Delta phase: a face-centered cubic hydride phase. A delta-prime phase has also been reported, formed below 240°C from the delta phase.
4. Epsilon phase: a face-centered tetragonal hydride phase with the ratio $c/z < 1$, extending beyond the delta phase to ZrH_2 . The epsilon phase is not a true equilibrium phase, and it appears as a banded, twin structure.

The two-phase delta plus epsilon region exists between $\text{ZrH}_{1.64}$ and $\text{ZrH}_{1.74}$ at room temperature, diminishes in width with increasing temperature, and closes at 455°C and $\text{ZrH}_{1.70}$. At higher temperatures, the delta and epsilon single-phase regions are separated by a single boundary sloping toward higher H/Zr ratios, reaching ZrH_2 at about 903°C. The transitions are postulated to be first order at the two-phase region and second order at the single-phase region.

When uranium is present, it appears to be partially rejected from solution during the hydriding process. The uranium which is

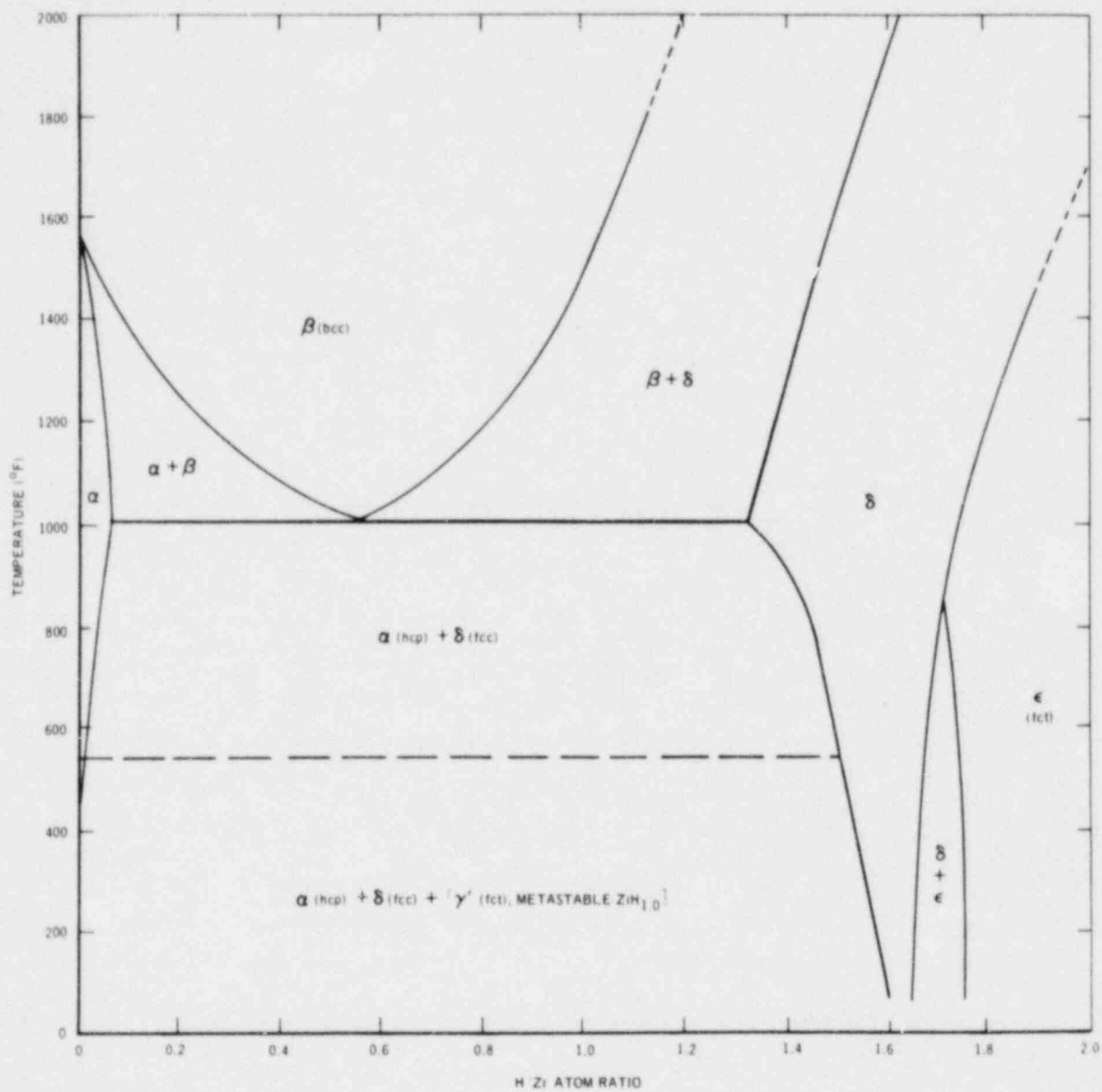


Fig. 2-4. Zirconium hydride phase diagram, showing boundary determination (from Ref. 19)

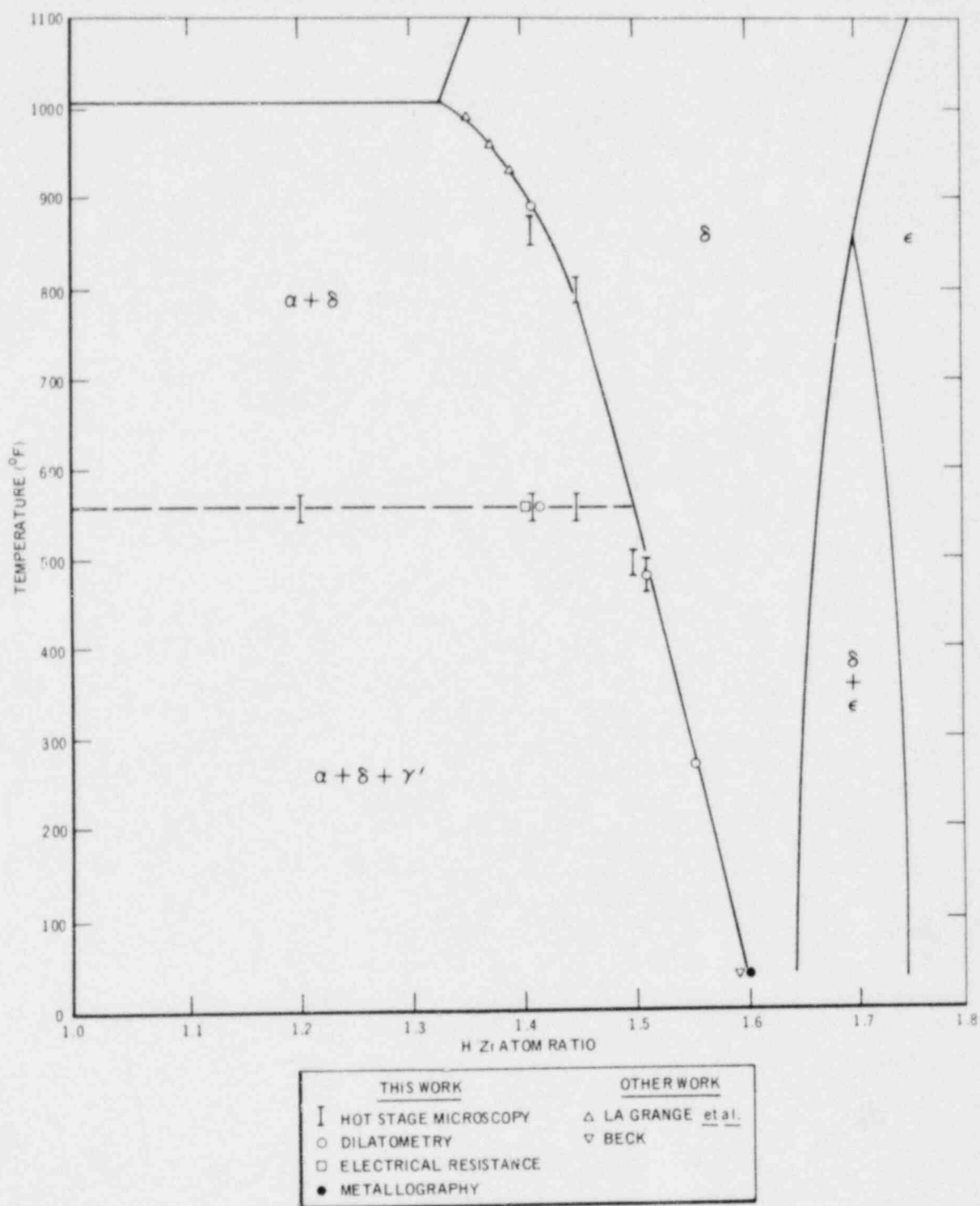


Fig. 2-5. Zirconium hydride phase diagram, enlargement of area under study (from Ref. 19)

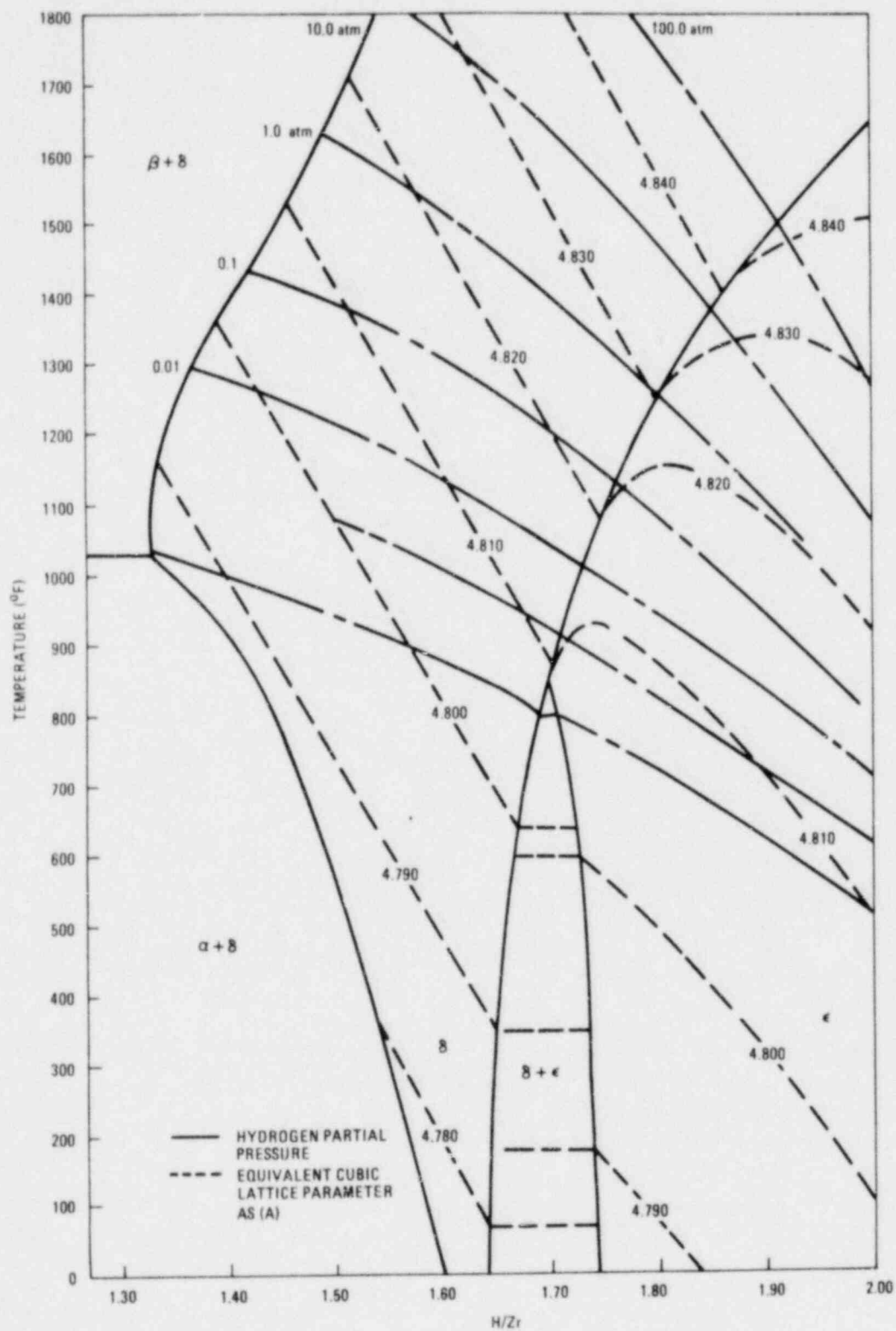
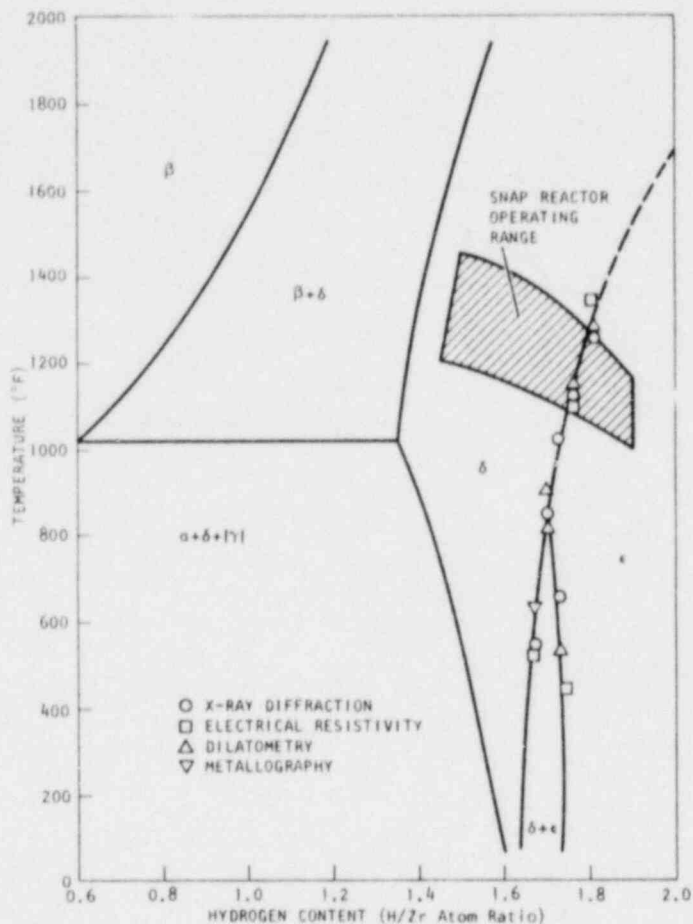
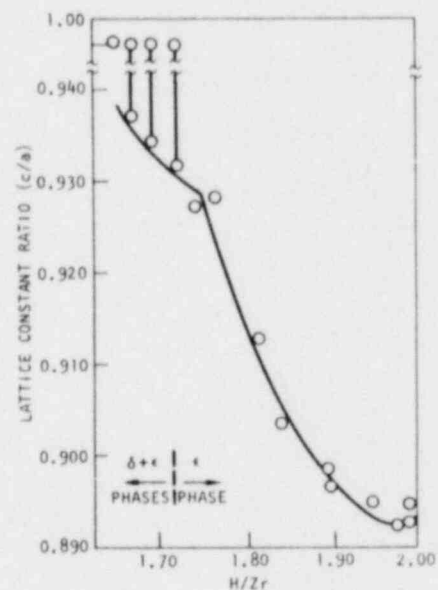


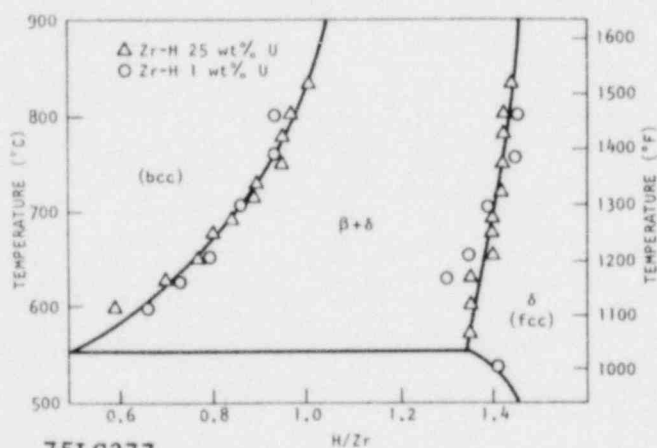
Fig. 2-6. Zirconium hydride phase diagram (from Ref. 13)



A. ZIRCONIUM-HYDROGEN
PHASE DIAGRAM



C. VARIATION OF DEGREE OF
TETROGONALITY OF ϵ HYDRIDE
WITH HYDROGEN CONTENT



B. δ AND $(\delta+\beta)$ ZIRCONIUM
HYDRIDE PHASE BOUNDARY

75LC377

EL-1611

Fig. 2-7. Zirconium-hydrogen phase relationships (from Ref. 20)

rejected is present as a fine, uniform dispersion. The effect of the uranium addition on the ZrH system is to shift all the phase boundaries of the ZrH diagram to slightly lower temperatures. For example, the eutectoid temperature is lowered from 547° to 541°C. The presence of erbium also has a more marked lowering of phase change temperature. No new phases and no uranium hydride have been detected (Ref. 21). At rather high uranium contents (25 to 50 wt %) the behavior with hydrogen was found to be a breakdown of the inter-metallic alloy. The zirconium reacted with the hydrogen giving poly-phase regions of uranium, zirconium, and zirconium hydride phases, mainly the cubic delta hydride. The phase boundaries of the ZrH diagram were relatively unaffected in the region of high hydrogen content, but the alpha and beta phases were markedly shifted. The main effect of the addition of uranium in the low hydrogen content region was to considerably increase the range of the alpha phase. Uranium hydride phases were not observed.

There is no generally accepted theoretical description of the structure of metal hydrides (Ref. 22). At present, two quite different theories are used to discuss metal hydrides. In one, the hydrogen is regarded as losing its electron to the conduction band of the metal structure, and as being present in the lattice as H^+ . This theory describes the transition metal hydrides as metallic or as alloys. The alternative theory considers that the hydrogen atom acquires an electron from the conduction band and is present as H^- . The depleted conduction band remains to give residual metallic bonding in the hydride and to account for the metallic properties. This theory describes the hydrides as ionic. It is possible that covalent bonding could be introduced into either theory, although few attempts have been made to do so. In any case, the small hydrogen atom would be expected to enter the tetrahedral sites in the usually close-packed metal structure. Nevertheless, most hydrides do not have their metal atoms

in the same position as in the parent metal. The solubility of hydrogen in zirconium above the eutectoid temperature was found to be increased by the presence of beta-stabilizing elements and decreased by alpha-stabilizers.

Oxygen concentrations of over 3.5 at. % in the hydride shift the two-phase boundaries ($\delta + \epsilon$) to lower H/Zr ratios, and the two-phase region becomes wider with increasing oxygen (Ref. 20). Reactor grade zirconium contains about 800 to 1000 ppm oxygen, and further oxygen contamination may occur during hydriding.

2.4. DISSOCIATION PRESSURES

The rates of hydriding and dehydriding of zirconium are markedly influenced (reduced) by the presence of surface oxide or nitride films. The surface films will, therefore, affect the measured hydrogen dissociation pressures unless precautions are taken to eliminate these films.

The hydrogen dissociation pressures of hydrides have been shown to be comparable in the alloys containing up to 75 wt % U (Ref. 23). The concentration of hydrogen is generally reported in terms of either weight percent or atoms of H/cm³ of fuel (N_H). The equilibrium dissociation pressures in the ZrH system are given in Figs. 2-8 and 2-9. In the δ region, the dissociation pressure equilibria of the zirconium-hydrogen binary may be expressed in terms of composition and temperature by the relation

$$\log P = K_1 + (K_2 \times 10^3)/T \quad ,$$

where $K_1 = -3.8415 + 38.6433 X - 34.2639 X^2 + 9.2821 X^3$.

$K_2 = -31.2982 + 23.5741 X - 6.0280 X^2$,

P = pressure, atm,

T = temperature, K,

X = hydrogen-to-zirconium atom ratio.

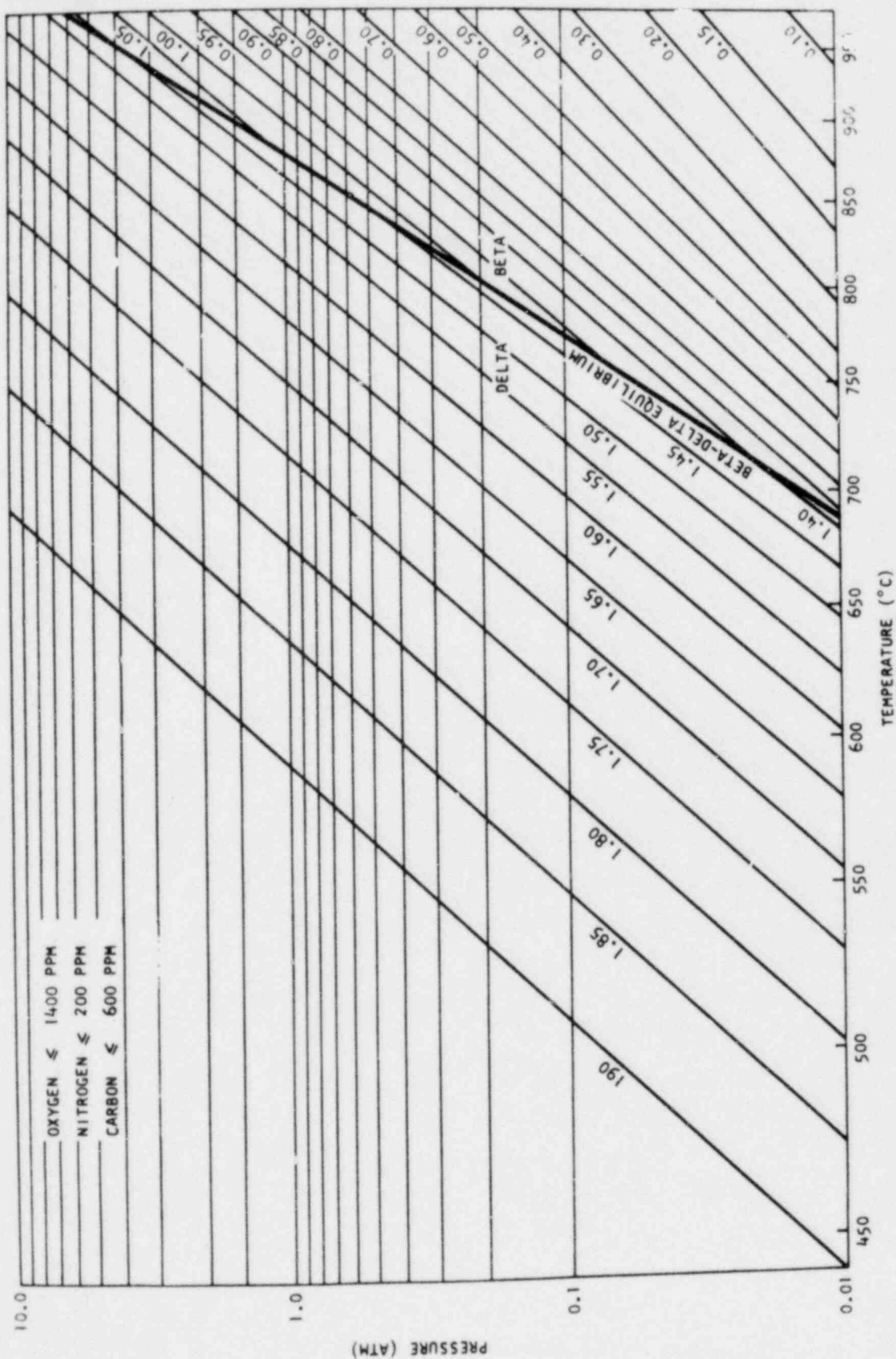
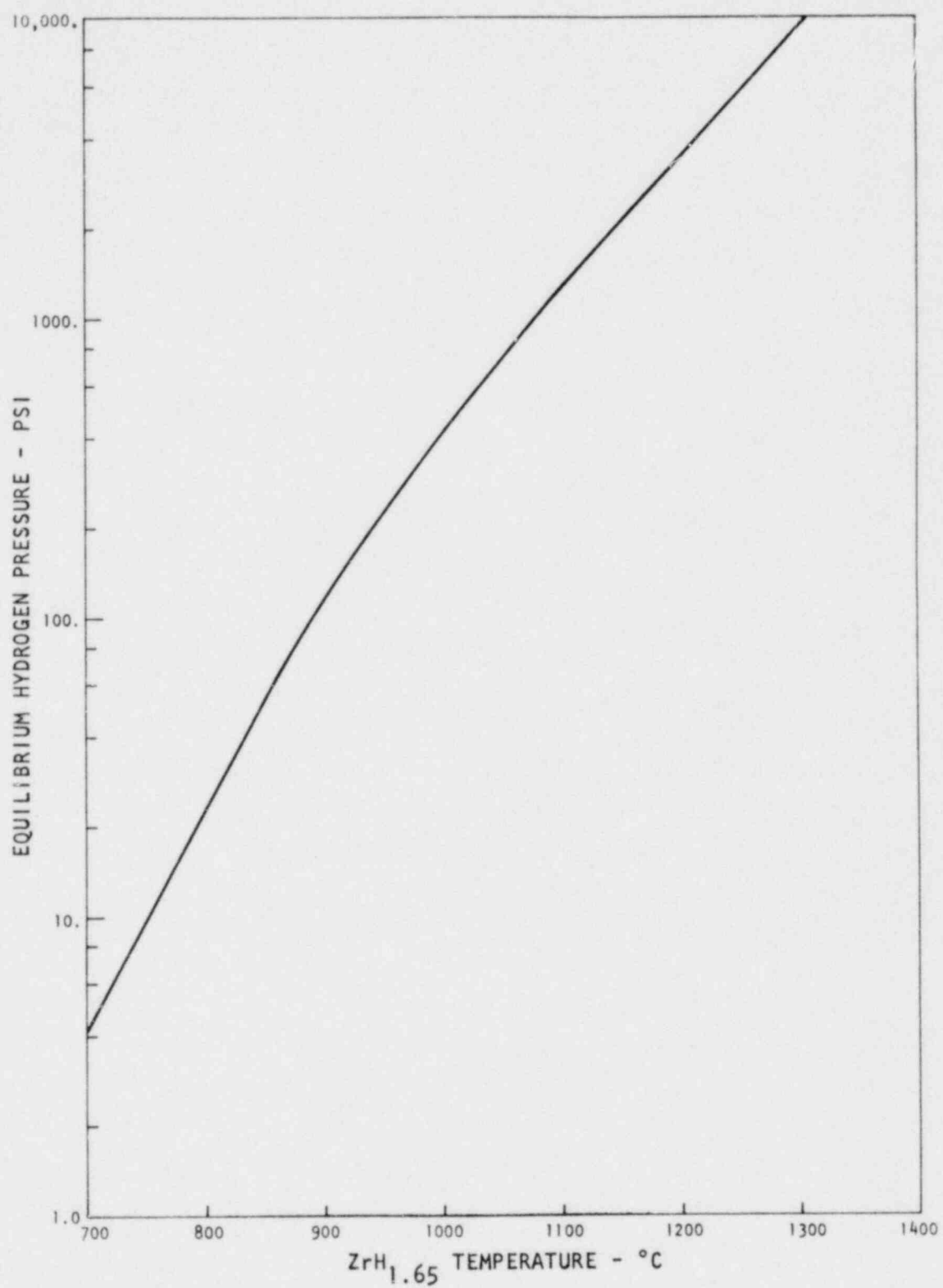


Fig. 2-8. Dissociation pressure isochores of zirconium hydride (expressed as H/Zr atom ratios) (from Ref. 23)



EL-1174

Fig. 2-9. Equilibrium hydrogen pressure over $\text{ZrH}_{1.65}$ versus temperature

The heat of solution of hydrogen in the delta hydrided phase decreases with increasing solute concentration, from -46.3 kcal/mole in delta of composition $\text{ZrH}_{1.4}$ to -37.7 kcal/mole in epsilon of composition $\text{ZrH}_{1.9}$ (Ref. 23). It is significant that no discontinuity in the function is in evidence throughout the entire delta-to-epsilon composition range, involving an H/Zr composition range of about 1.4 through 1.9. This is compatible with the transition from fcc-delta to fct-epsilon, involving a continuous anisotropic expansion of the cubic phase. The isochores of the delta and epsilon regions of the ZrH system exhibit a progressively increasing change in spacing with increasing hydrogen concentration. Any deviation from this type or progression is attributed to significant contamination of the binary with oxygen, nitrogen, carbon, etc., to form a ternary or higher-order alloy system.

The higher-hydride compositions ($\text{H/Zr} > 1.5$) are single-phase (delta or epsilon) and are not subject to thermal phase separation on thermal cycling. For a composition of about $\text{ZrH}_{1.6}$, the equilibrium hydrogen dissociation pressure is 1 atm at about 760°C. The absence of a second phase in the higher hydrides eliminates the problem of large volume changes associated with phase transformations at approximately 540°C in the lower hydride compositions. Similarly, the absence of significant thermal diffusion of hydrogen in the higher hydrides precludes concomitant volume change and cracking. The clad material of stainless steel or nickel alloys will provide a satisfactory diffusion barrier to hydrogen at long-term (several years) sustained cladding temperatures below about 300°C.

The equilibrium dissociation pressures in the H/Zr composition range of 1.4 to 1.7 at temperatures up to 1300°C have been measured (Ref. 3). The results for an H/Zr range of 1.55 to 1.7 agree closely with the values obtained from extrapolation of the reported data which extend to 950°C. However, the data for an H/Zr range of 1.4 to 1.5 indicate that the hydrogen dissociation pressures for these compositions are considerably lower than the values extrapolated from the temperatures below 950°C, probably as a result of phase changes at the elevated temperatures. For example, at

the H/Zr ratio of 1.5, the measured dissociation pressure at 1100°C is about 9 atm versus the extrapolated value of 25.2 atm and at 1200°C is about 17 atm measured versus 60 atm extrapolated.

The influence of carbon on the dissociation pressures of hydrogen in carbon-modified ZrH has been measured (Ref. 24). The dissociation pressures were found to be predictably higher than the dissociation pressures of the carbon-free hydrides. The hydrogen dissociation pressures are expressed as a function of temperature and composition as follows:

$$P = K \exp (-\Delta H_a / RT) \quad ,$$

where the value of K is governed by composition. The carbon is associated with zirconium on a 1:1 ratio.

The hydrogen dissociation pressure for fuel with H/Zr ratios of 1.7 to 1.9 is given by

$$\log P = 10.44 (H/Zr) - 10.47 - 8538/T \quad ,$$

where the dissociation pressure P is in atm and the temperature T is in K.

The association of zirconium with carbon necessitates an increase in the H/Zr ratio in order to maintain the required N_H , resulting in an increase in the hydrogen dissociation pressure (Refs. 24 through 27). The equilibrium dissociation pressures are then given by

$$\ln P = A_0 + A_1 (10^4/T_K) \quad ,$$

where

$$A_0 = B_0 + B_1 (H/Zr) + B_2 (H/Zr)^2 + B_3 (H/Zr)^3 ,$$

$$A_1 = C_0 + C_1 (H/Zr) + C_2 (H/Zr)^2 + C_3 (H/Zr)^3 ,$$

$$H/Zr \text{ (effective)} = 90.496 \frac{\text{wt \% H}}{\text{wt \% Zr} - 7.5947 \text{ wt \% C}} ,$$

$$\text{wt \% Zr} = 100 - (\text{wt \% H} + \text{wt \% C} + \text{wt \% U}) ,$$

$$H/Zr \text{ (total)} = 90.496 \frac{\text{wt \% H}}{100 - (\text{wt \% H} + \text{wt \% C} + \text{wt \% U})} .$$

An equivalent approach is to subtract the Zr atoms which form ZrC and treat the remaining Zr as hydrided with standard characteristics of ZrH for the resulting H/Zr ratio.

A temperature excursion in an accident situation would increase the hydrogen pressure in the cladding, as indicated by the dissociation pressure curves. This would govern the design of the cladding (wall thickness, material, and allowable strain) in terms of the maximum hydrogen pressure to be accommodated at the maximum temperature during an excursion.

2.5. HYDROGEN MIGRATION

Under nonisothermal conditions, hydrogen migrates to lower-temperature regions from higher-temperature regions. The equilibrium dissociation pressure obtained when the redistribution is complete is lower than the dissociation pressure before redistribution. The dimensional changes of rods resulting from hydrogen migration are of minor importance in the delta and epsilon phases.

The results of studies on the thermal migration of hydrogen in ZrH have been described (Refs. 28, 29). No significant hydrogen redistribution was observed in the delta- or epsilon-phase hydrides. In the lower hydrides, however, extensive migration of hydrogen took place.

The kinetics of hydrogen migration in delta zirconium hydride have been measured in the temperature range of 650° to 800°C (Ref. 29). The hydrogen absorption follows a parabolic time law, and the rate constant is proportional to the concentration difference and to the square root of the diffusion constant. The temperature dependence of diffusion in the delta phase is given by

$$D = 0.25 \exp(-17800/RT) \quad .$$

The diffusion of hydrogen in zirconium hydride was found to be independent of concentration.

"Thermal migration stresses" arise when hydrogen migrates from the higher to the lower temperature regions of the fuel, causing the colder region to expand and the hotter region to contract. The consequences (Ref. 30) of this redistribution of hydrogen are: "This results in a 'migration stress' which is in the opposite sign (or direction) of the thermal stress. Since this process is time-dependent, a temperature gradient in Zirconium hydride will first cause a thermal stress which is slowly relieved by hydrogen migration. The final stress on the material will be that due to the superposition of the two phenomena, with the equilibrium migration stress believed to be somewhat larger in absolute magnitude." The brittle nature of zirconium hydride at the lower temperatures makes it susceptible to thermal stress cracking.

If the radial temperature gradient on the fuel rod is assymmetric, bowing of the rod will occur. The SNAP reactor experience (Ref. 30) indicated that "if during this redistribution (of hydrogen) and bowing change the thermal gradients are altered, as would be the case in an operating reactor, the conditions for sustained cycling are obtained Anomalous oscillations were observed in the SNAP-8 reactor power level and local outlet coolant temperatures. These oscillations continued

with a decreasing magnitude and frequency for about the first 1500 hr of operation. The oscillatory behavior was probably due to the clustering of fuel elements under a thermal gradient, followed by an abrupt declustering caused by the rehydriding of the fuel rod which applies a force in the opposite direction. The diffusion of hydrogen from the hotter to colder regions of the fuel rod make it act as if it had a delayed, negative coefficient of thermal expansion."

The diffusion coefficient of hydrogen in the delta hydride has been measured (Ref. 13). The diffusion rate equation (650 to 900°C, H/Zr = 1.5 to 1.8) is: $D = 1.3 \times 10^{-2} \exp(-12,690/RT)$. No concentration dependence was found. Neither carbon nor uranium had any effect on the hydrogen diffusion. For example, at 650°C, $D = 0.7 \times 10^{-4} \text{ cm}^2/\text{sec}$. The hydrogen redistribution will take place fairly rapidly in the central high temperature regions and much more slowly near the cooler surface regions. Hence, the volume changes and the concomitant stresses will be applied relatively slowly in the more brittle cooler regions and would be accommodated, as indicated by actual experience.

Measurements and calculations have been reported of hydrogen loss from hydrided 10 wt % U-Zr fuel elements (3.2 cm in diameter by 2.54 cm. long) which were rapidly heated by induction to temperatures near the melting point (Refs. 31, 32). Results indicated that within about 75 sec the surface temperature in a nonoxidizing atmosphere reached 930° to 970°C (1700° to 1780°F) with only minor hydrogen evolution. Abruptly thereafter, the surface was observed to crack parallel with the cylindrical axis, with strong outgassing rates, and the temperature dropped. After a few seconds, the temperature again began to rise and outgassing continued. After about 3 min at surface temperatures of 1100° to 1105°C (2010° to 2020°F), the specimen was cooled. Subsequent analysis showed large amounts of residual hydrogen. In another series of tests, temperatures up to 1900°C (3400°F) were reached before power was shut off. In these tests, almost all the hydrogen was driven off. The volume of

the sample was found to have decreased, and the surface cracks visibly healed as the temperature rose above 1100°C (2000°F).

2.6. HYDROGEN RETENTION

In oxidizing environments, the protective oxide films formed on the hydride surfaces can lower the rate of hydrogen losses. In the KNK reactor (West Germany), unclad zirconium hydride was exposed to flowing sodium at 550°C for several thousand hours (Ref. 29). The hydrogen losses were about equivalent to losses from 0.2-mm-thick stainless-steel-clad hydride, because the oxygen in the sodium oxidized the zirconium hydride to form a low-permeability oxide film. Hydrogen loss was estimated to be about 10% in 20 yr of operation with bare or clad zirconium hydride into the flowing sodium coolant. This would result in a loss of reactivity of 1.5%.

The rates of hydrogen loss through 250- μ m-thick stainless steel cladding are shown in Fig. 2-10 (Ref. 18). A 1% loss of hydrogen per year occurs at about 500°C (900°F) clad temperature. The hydrogen permeabilities for a number of clean metals and alloys are shown in Fig. 2-11. Glass-enamel-coated metal cladding (about 76- μ m-thick glass coating) has very low permeabilities (about 10% of molybdenum) and has been used successfully in the SNAP reactor fuel elements at temperatures up to 700°C.

2.7. DENSITY

The density of ZrH decreases with an increase in the hydrogen content, as shown in Figs. 2-12 and 2-13. The density change is quite high up to the delta phase ($H/Zr = 1.5$) and then changes little with further increases in hydrogen (Ref. 33). The bulk density of massively hydrided zirconium is reported to be about 2% lower than the x-ray density.

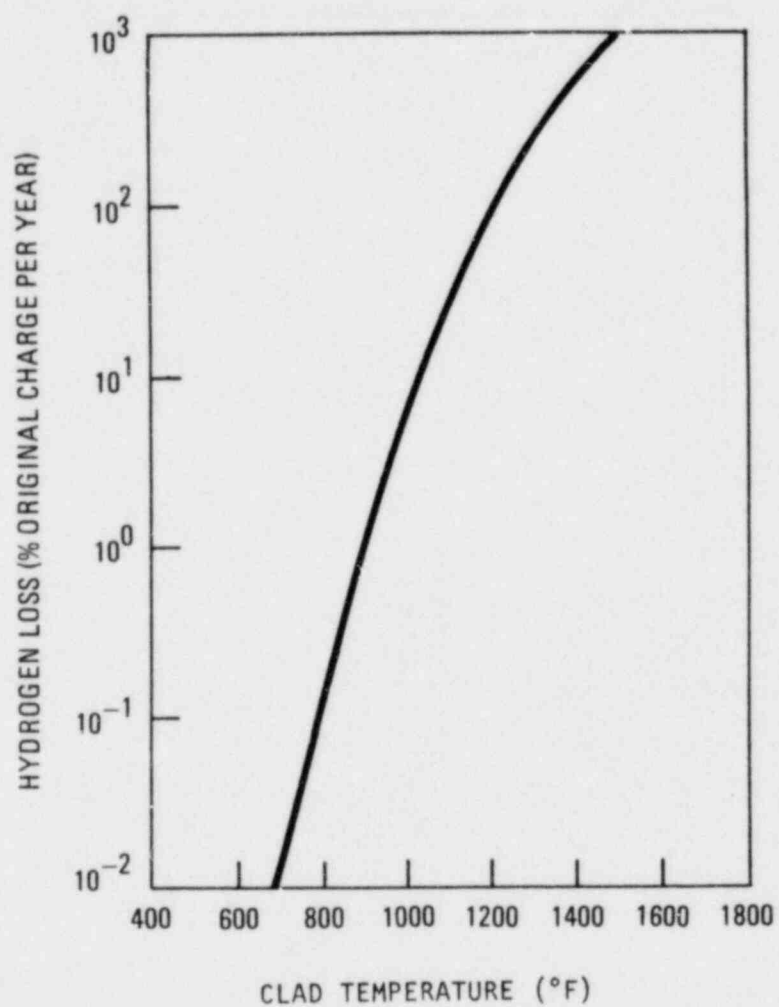


Fig. 2-10. Hydrogen loss rate through 10-mil-thick stainless steel moderator can (from Ref. 18)

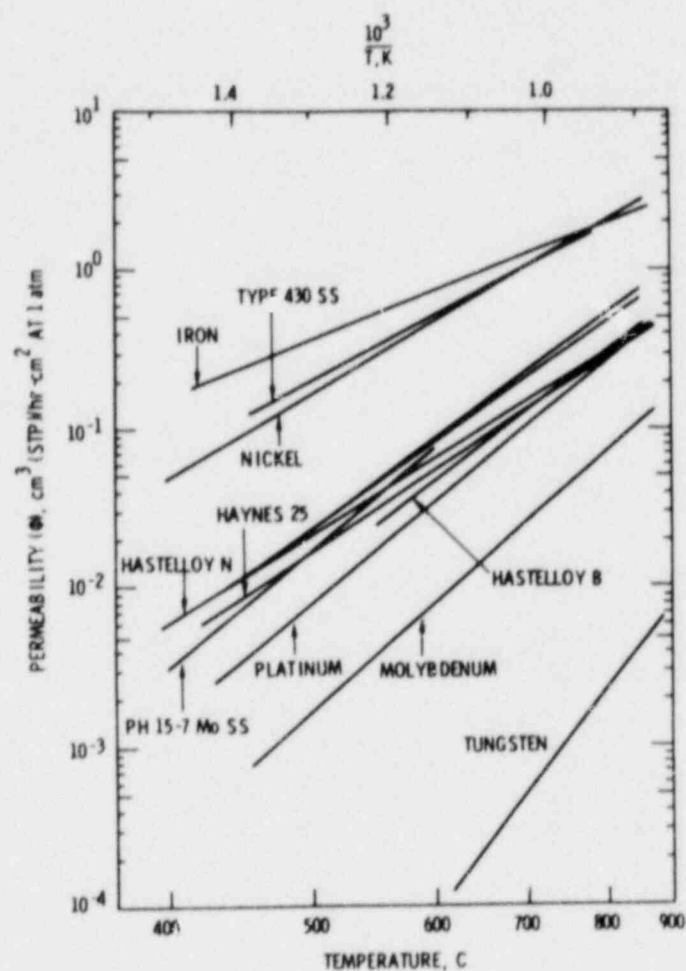


Fig. 2-11. Permeability of various metals to hydrogen (1-mm-thick metal) (from Ref. 17)

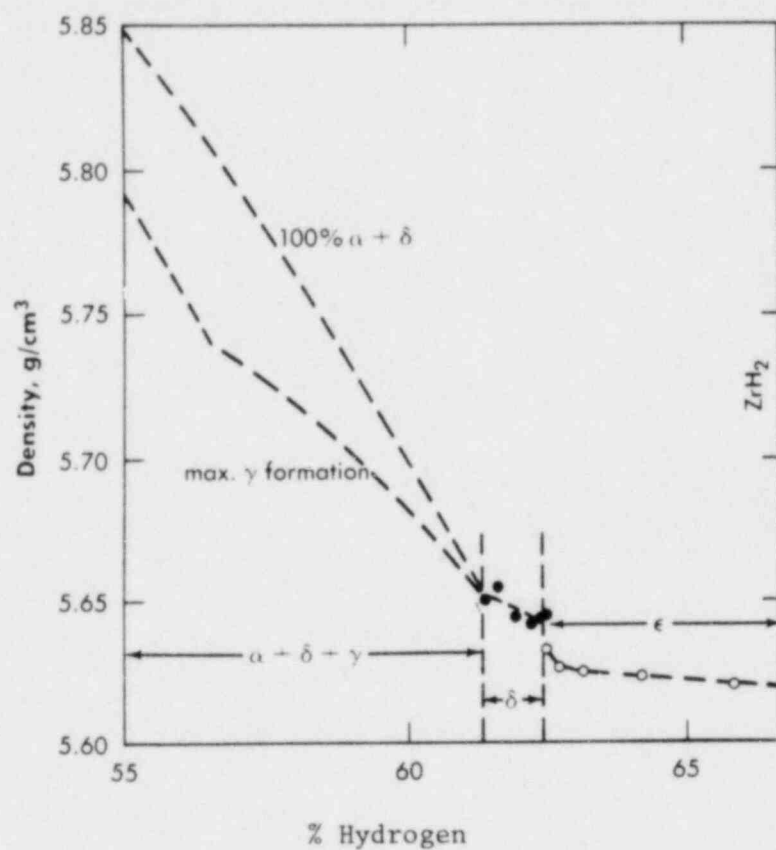


Fig. 2-12. Density of delta and epsilon phases of zirconium hydride as determined by x-ray diffraction (from Ref. 12)

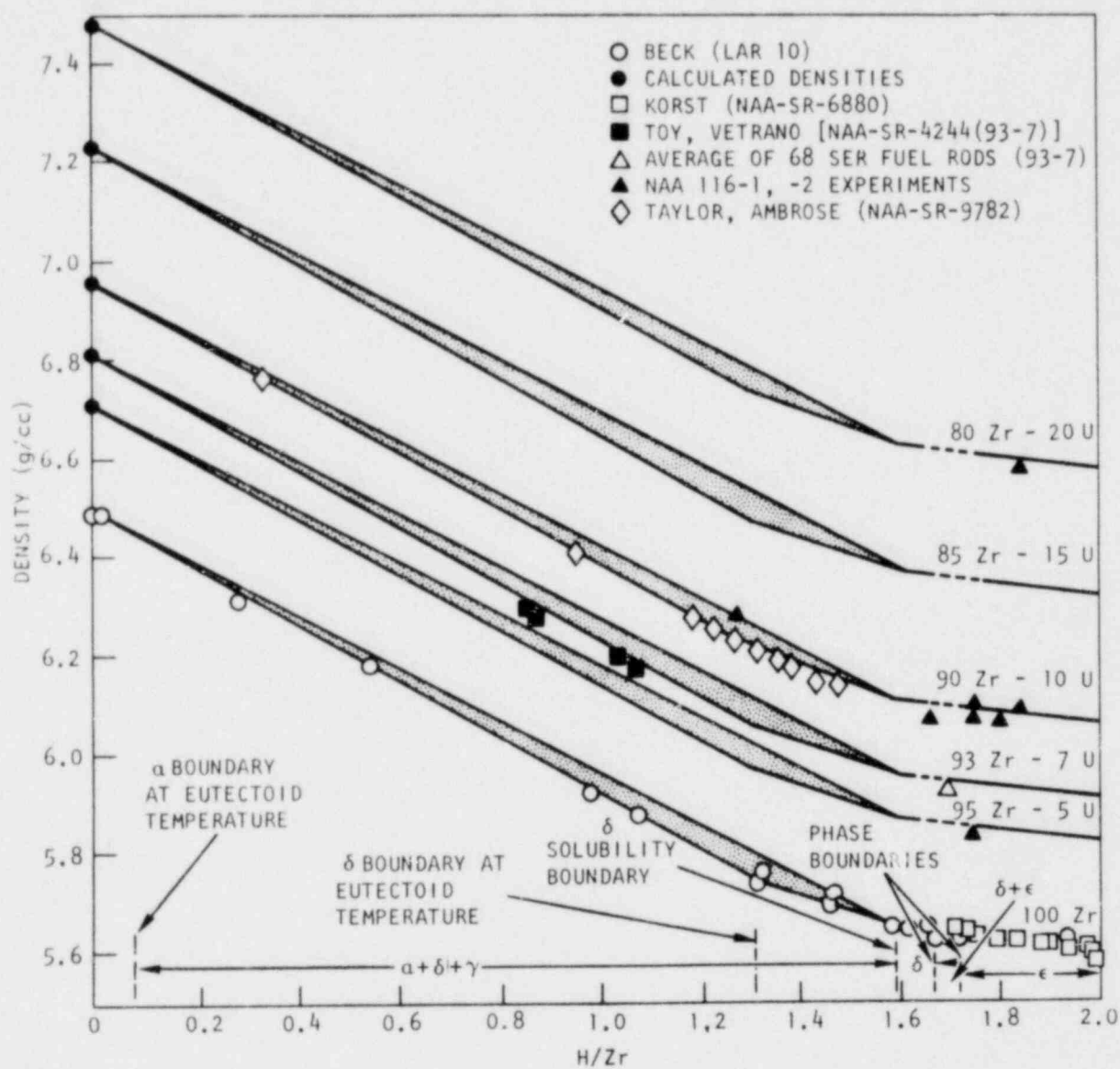


Fig. 2-13. Density diagram (from Ref. 46)

For hydrogen to zirconium ratios, x , of less than 1.6 the density of ZrH_x used for TRIGA design calculation is

$$\rho_{ZrH} = 1./(.1541 + .0145 X)$$

and for X greater than or equal to 1.6

$$\rho_{ZrH} = 1./(.1706 + .0042 X)$$

The density of uranium-zirconium hydride is

$$\rho_{UZrH} = 1./(w_U/\rho_U + w_{ZrH}/\rho_{ZrH})$$

where w_U , w_{ZrH} = weight fraction of uranium and zirconium hydride respectively and ρ_U = uranium density (19.07 gm/cm^3).

2.8. THERMAL CONDUCTIVITY

Thermal conductivity measurements have been made over a range of temperatures (Refs. 34, 35). A problem in carrying out these measurements by conventional methods is the disturbing effect of hydrogen migration under the thermal gradients imposed on the specimens during the experiments. This has been minimized by using a short-pulse heating technique to determine the thermal diffusivity and hence to permit calculation of the thermal conductivity. A value of $0.042 + 1.79 \times 10^{-5} T$ cal/sec-cm-°C is used for the thermal conductivity for design calculations.

Measurements have been made (Ref. 36) of the thermal diffusivity of uranium-zirconium hydride in which the uranium content was 8.5, 30 and 45 percent by weight. The data from these measurements, in conjunction with the best available data for density and specific heat, was used to determine the thermal conductivity of these materials.

The thermal conductivity so determined was found to be both independent of temperature and uranium content and is

$$\begin{aligned} k &= 0.18 \pm 0.009 \text{ watts/cm } ^\circ\text{C} \\ &= 0.043 \pm 0.00215 \text{ cal/sec-cm-}^\circ\text{C} \end{aligned}$$

The temperature independence does not agree with measurements made by others (Refs. 34, 35). Nevertheless, assuming that the information contained here is correct, the maximum temperature of a TRIGA fuel element operating at maximum power density would be only about 50°C higher than that calculated using the older temperature dependent thermal conductivity relationship.

2.9. HEAT CAPACITY

The heat content of zirconium hydride as a function of temperature and composition (ZrH_x) is approximated well by the following relationship (Refs. 37 through 39):

$$\begin{aligned} (\text{H}-\text{H}_{25})_{\text{ZrH}_x} &= .03488T^2 + [34.446 + 14.8071 (X - 1.65)] T \\ &\quad - 882.95 - 370.18 (X - 1.65) \text{ joules/mole} \end{aligned}$$

where T is in $^\circ\text{C}$

The specific heat of $\text{ZrH}_{1.6}$ is

$$C_p = (.06976 T + 33.706) M \text{ joules/gm } ^\circ\text{C}$$

where M = the molecular weight of $\text{ZrH}_{1.6} = 92.83 \text{ gms/mole}$

The specific heat of uranium is

$$C_p = (1.305 \times 10^{-4} T + .1094) \text{ joules/gm } ^\circ\text{C}$$

The specific heat of uranium-zirconium hydride is taken to be

$$C_{p(\text{UZrH})} = W(\text{U})C_{p(\text{U})} + W(\text{ZrH})C_{p(\text{ZrH})} ,$$

The volumetric specific heat of 8.5 wt % U-ZrH_{1.6} is calculated to be:

$$C_p = 2.04 + 4.17 \times 10^{-3} T \text{ W-sec/cm}^3 \text{ } ^\circ\text{C (from } 0^\circ\text{C)} .$$

The specific heat curves for the delta and epsilon phases are shown in Fig. 2-14. The volumetric heat content of 8.5 wt % U-ZrH_{1.6} alloy is calculated to be:

$$H - H_{25} (8.5 \text{ U-ZrH}_{1.6}) = 2.08 \times 10^{-3} T^2 + 2.04T - 52.2 \text{ W-sec/cm}^3 .$$

2.10. THERMAL EXPANSION

The thermal expansion of zirconium hydride has been measured using both dilatometric and x-ray diffraction techniques. The expansion coefficient increases with increasing temperature. The data for the delta and epsilon phases have been fitted to an equation of the form (Ref. 17):

$$\frac{\Delta l}{l} = -0.288 \times 10^{-3} + 6.24 T + 7.34 \times 10^{-3} T^2 ,$$

where T is in $^\circ\text{C}$ and $\Delta l/l$ is the fractional change in length. The average expansion coefficient for the delta phase over the range of 200° to 850°C is $14.2 \times 10^{-6}/^\circ\text{C}$. Experimental data over the range of 93° to 650°C are given in Table 2-1.

In the presence of thermal gradients in ZrH rods, hydrogen composition gradients will be created in accordance with the phase-temperature-composition equilibria of the ZrH system (Ref. 30) as defined in

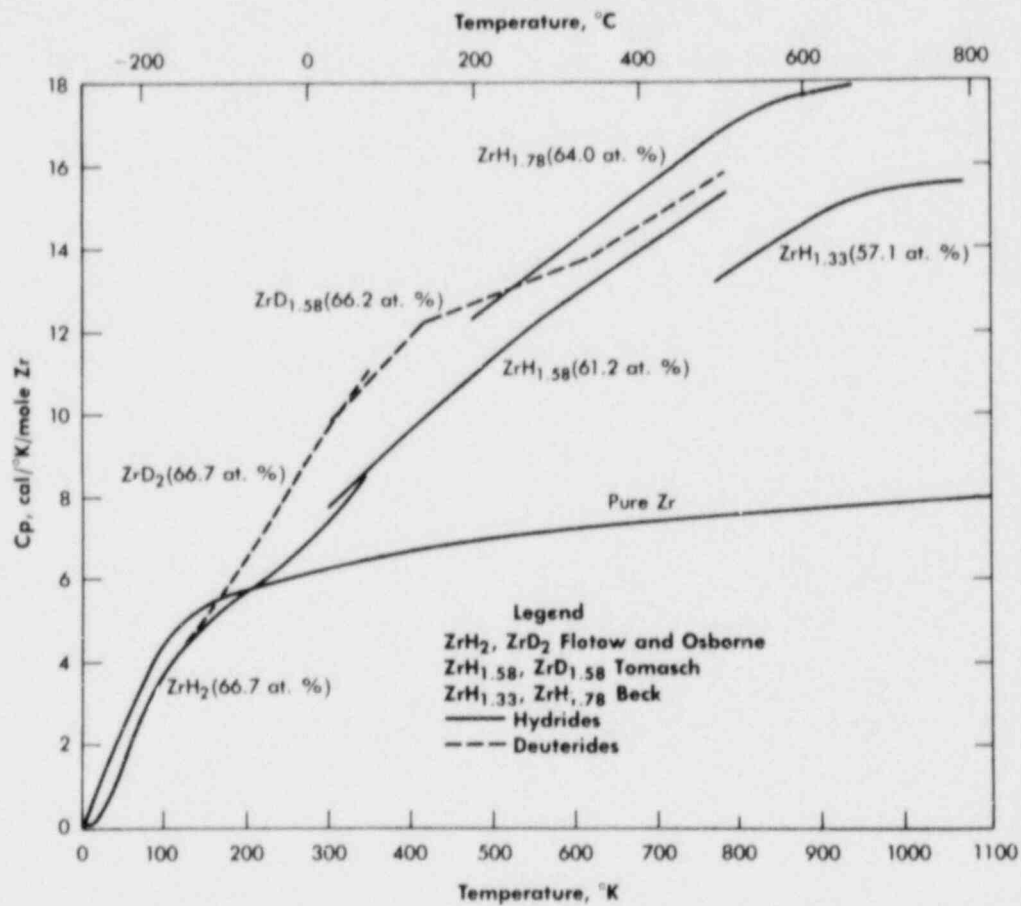


Fig. 2-14. Specific heat curves for delta and epsilon phases (from Ref. 12)

TABLE 2-1
THERMAL EXPANSION^(a)

Material	Total Expansion from Room Temperature, $\mu\text{m}/\text{cm}$				
	93°C	205°C	310°C	540°C	650°C
Crystal bar zirconium	1.2	8.5	25.2	34.0	44.5
Zirconium hydride, H/Zr - 1.7	3.3	11.7	35.9	51.1	68.8

(a) Taken from Ref. 18.

Fig. 2-15. This will result in the unusual phenomenon of a negative thermal expansion because

. . . the hydrogen will redistribute, enriching the cold or concave side and depleting the hot or convex side of a rod [(i.e., the lower temperatures correspond to a greater relative volume than higher temperatures)]. . . . This will result (after a period of time depending on the hydrogen diffusion rate) in the cold side having larger dimensions than the hot side, and, therefore, a reversal of the configuration with the cold side convex and the hot side concave. Furthermore, if during this redistribution and bowing change the thermal gradients are altered, as would be the case in an operating reactor, the conditions for sustained cycling are obtained - (from Ref. 30, p. 3).

This phenomenon was verified experimentally, as shown in Fig. 2-16.

The thermal expansion coefficient has been measured (Ref. 36) for uranium-zirconium hydride containing 45 percent by weight uranium and compared to the coefficient for 8 to 12 weight percent uranium. For a maximum power density TRIGA fuel element, the maximum radial expansion would be about 0.6% for 45 wt % fuel as opposed to 0.5% for 8 to 12 wt % fuel.

The coefficient of thermal expansion is strongly dependent upon temperature. A good fit to the expansion data is obtained by use of a second degree polynomial in temperature. For the SNAP data (Ref. 40) the expansion coefficient is

$$\frac{\Delta l}{l} = 4.52 \times 10^{-6} + 19.25 \times 10^{-9} T (^{\circ}\text{C})^{-1}$$

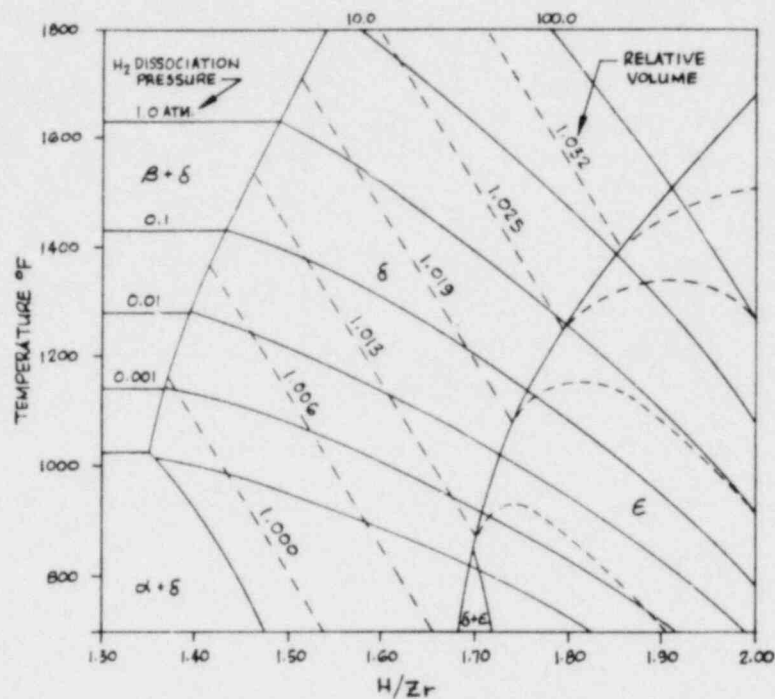


Fig. 2-15. Zirconium hydride phase diagram with isobars and isometrics (from Ref. 32)

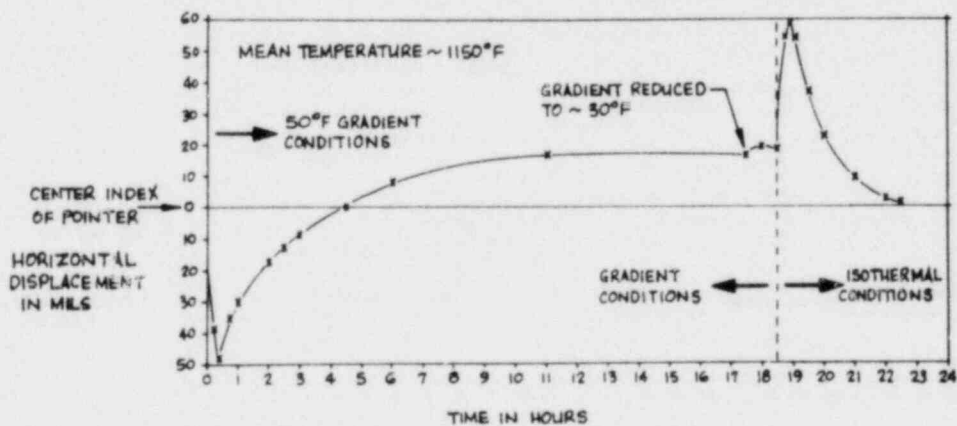


Fig. 2-16. Bow of a UZrH rod resulting from an asymmetric thermal gradient (from Ref. 30)

Two specimens of 45 wt % uranium-zirconium hydride were thermally cycled over 100 times from room temperature to 800°C. The linear expansion as a function of temperature was measured with a dilatometer. Although a phase transformation takes place at about 650°C which results in an isothermal density change a least square fit to the data from the first and last thermal cycle of both specimen showed a maximum deviation of measured values to the fit of less than 10%. From these measurements, the expansion coefficient for 45 wt % $\text{UZrH}_{1.6}$ is

$$\frac{\Delta l}{l} = 7.38 \times 10^{-6} + 15.1 \times 10^{-9} T (\text{°C})^{-1} .$$

2.11. MECHANICAL PROPERTIES

The mechanical properties of ZrH are difficult to measure because of its brittle nature. However, at elevated temperatures ZrH exhibits significant ductility and creep deformation. The creep strength is markedly influenced by the structure, as shown in Fig. 2-17 (Refs. 17, 41, 42). The beta phase has a much lower creep strength than the delta phase.

The temperature limit for ZrH in the reactor stems from the outgassing of hydrogen from the ZrH_x and the subsequent stress produced in the cladding material. The strength of the cladding as a function of temperature can set the upper limit on the ZrH temperature.

The tensile strengths and elongations of zirconium hydride are shown in Fig. 2-18. The presence of minor constituents such as carbon and oxygen also has a marked effect on the mechanical properties.

The dynamic elastic modulus of $\text{ZrH}_{1.6}$ was measured at room temperature as 63,000 MPa. This value decreases to about 41,000 MPa at 650°C (Ref. 17).

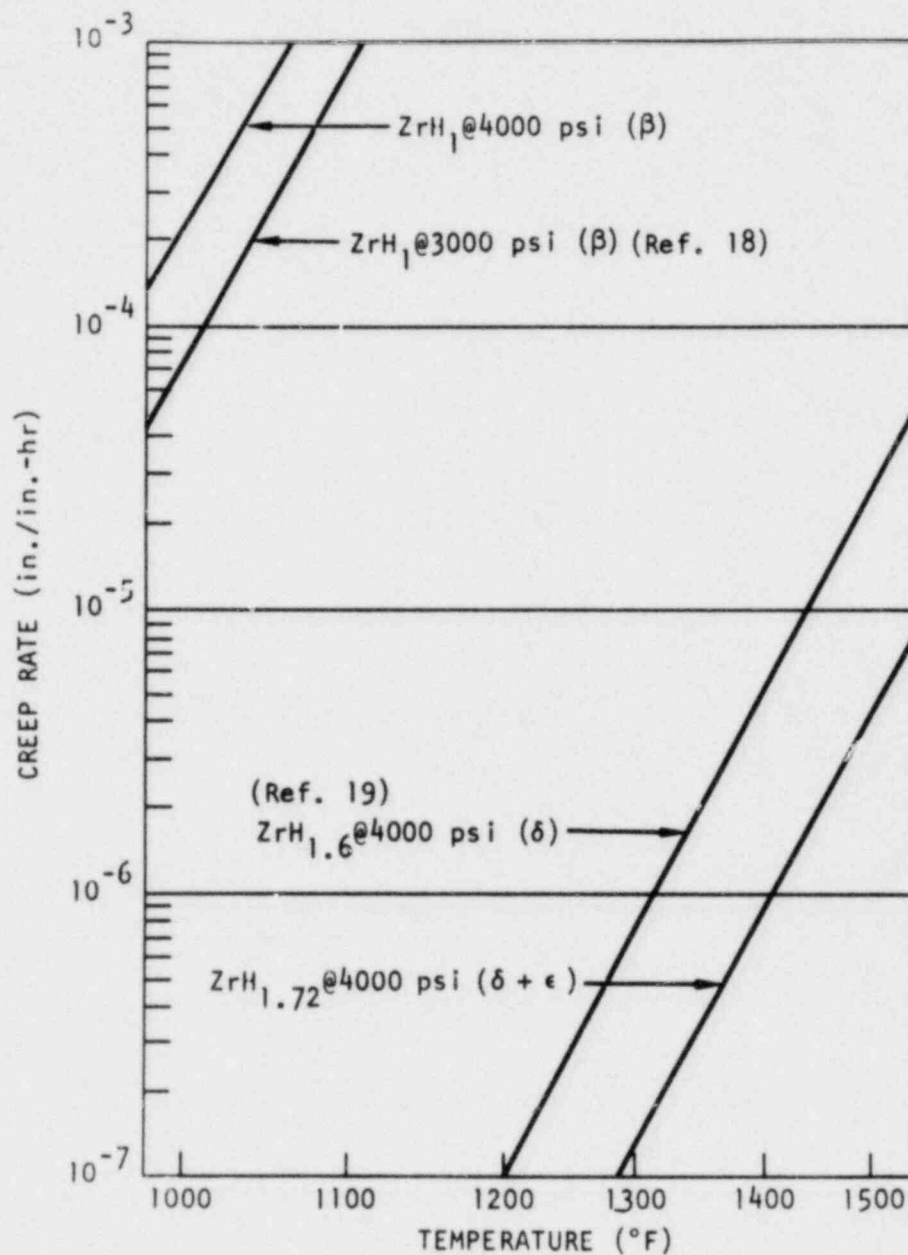


Fig. 2-17. Creep properties of zirconium hydride; comparison of β with δ and $\delta + \epsilon$ phase material (from Refs. 41, 42)

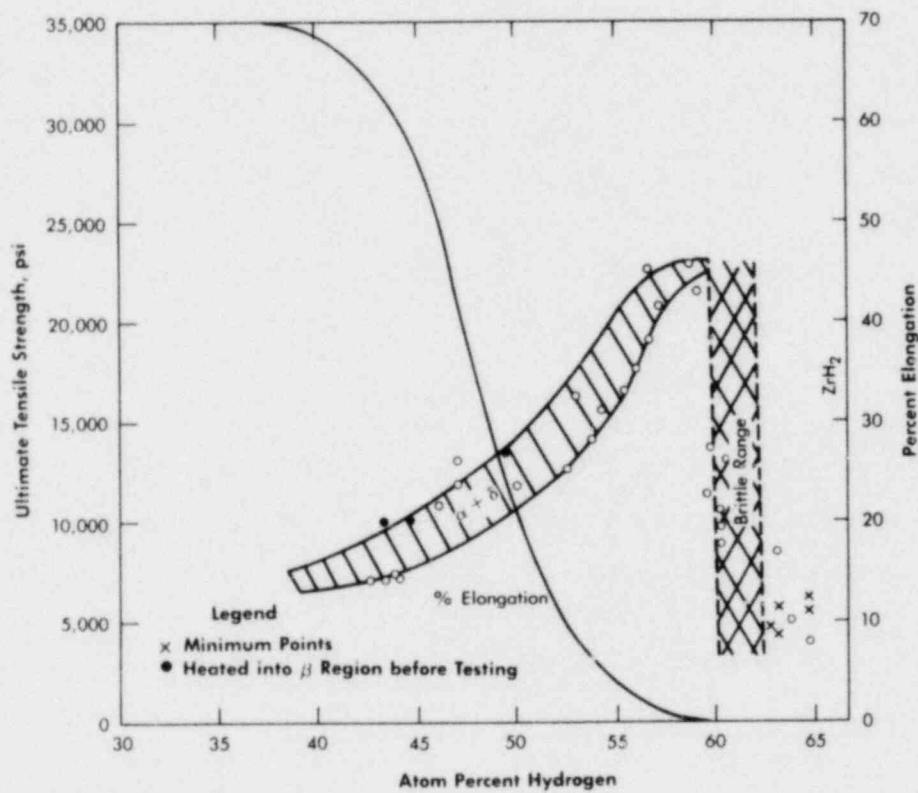


Fig. 2-18. Ultimate tensile strength and percent elongation of zirconium hydride at 600°C (from Ref. 12)

2.12. CORROSION PROPERTIES

Zirconium hydride has a relatively low reactivity in water, steam, and air at temperatures up to about 600°C (Ref. 18). Massive zirconium hydride has been heated in air for extended periods of time at temperatures up to 600°C with negligible loss of hydrogen. An oxide film forms which inhibits the loss of hydrogen.

The hydride fuel has excellent corrosion resistance in water. Bare fuel specimens have been subjected to a pressurized water environment at 570°F and 1230 psi during a 400 hr period in an autoclave (Ref. 8). The average corrosion rate was 350 mg/cm²-month weight gain, accompanied by a conversion of the surface layer of the hydride to an adherent oxide film. The maximum extent of corrosion penetration after 400 hr was less than 2 mils.

In the early phases of development of the TRIGA fuel, water-quench tests were carried out from elevated temperatures (Ref. 1). Fuel rods (1-in. diam) were heated to 800°C and end-quenched to test for thermal shock and corrosion resistance. No deleterious effects were observed. Also, a 6-mm diam fuel rod was heated electrically to about 800°C and a rapid stream of water was sprayed on it; no significant reaction was observed. Small and large samples were heated to 900°C and quenched in water; the only effect observed was a slight surface discoloration. Finely divided U-ZrH powder was heated to 300°C and quenched in 80° water; no reaction was observed. Later, these tests were extended to temperatures as high as 1200°C, in which tapered fuel rods were dropped into tapered aluminum cans in water. Although the samples cracked and lost hydrogen, no safety problem arose in these tests. Recently, the low-enriched TRIGA fuels have been subjected to water-quench safety tests at General Atomic (Ref. 43). The result of these tests have been described as follows.

Quench tests were performed on 20%-enriched TRIGA fuel samples (45 wt % uranium, 53 wt % zirconium, 1 wt % erbium, 1 wt % hydrogen) to simulate cladding rupture and water ingress into the TRIGA reactor fuel rods during operation.

The 12.9-mm diam by 12- to 18-mm long TRIGA fuel samples, which were inductively heated and quenched in water from temperatures ranging from 800° to 1200°C, showed remarkably satisfactory response to the test conditions. Minor cracking and small increases in density occurred in some samples. Hydrogen loss was accompanied by surface oxidation in all samples. Test results on samples quenched from approximately 1100°C were variable; these variations were at first believed to have been caused by differences in homogeneity of the fuel. Minor cracking, volume shrinkage, loss of hydrogen, and surface oxidation occurred in some samples, while other samples exhibited localized melting when heated to a measured temperature of 1050°C. The localized melting was caused by eutectics formed from reaction of the Inconel-600 thermocouple sheath with the fuel sample. Samples quenched from 1200°C showed variable behavior only because one sample contacted and reacted with the tantalum susceptor originally used for the inductive heating. The second sample showed very satisfactory behavior. For the tests where the fuel was heated to 800° and 1000°C, the sheathed thermocouple was inserted directly in contact with the surfaces of the hole. A molybdenum cup was inserted in the hole in the fuel specimen to prevent reaction with the Inconel-600 thermocouple sheath and the fuel at temperatures above 1100°C.

Quench testing at 800° and 1000°C resulted in no unusual occurrences for hold times of up to 3 min at temperature. However, initial tests at temperatures above 1050°C resulted in some localized melting of the fuel when the Inconel-sheathed thermocouple was in direct contact with the fuel. These observations indicate that the localized melting was the result of fuel reactions with the Inconel-600

thermocouple sheath, rather than with inhomogeneities in the fuel. Inconel-600 has a composition whose major constituents in wt % are 72 nickel, 14-17 chromium, and 6-10 iron. Low melting eutectics between uranium and the constituents occur as follows: nickel 740°C, chromium 859°C, and iron 725°C. The melting points of the eutectics between zirconium and the constituents are as follows: nickel 961°C, chromium 1300°C, and iron 934°C.

The test samples were characterized and compared with as-fabricated control samples by performing visual examination, dimensional and weight measurements, vacuum fusion analysis for hydrogen content, electron microprobe analysis for major constituents, and metallographic examination. The results are shown in Table 2-2 and Fig. 2-19.

The following conclusions can be drawn from quench tests from temperatures ranging from 800° to 1200°C on TRIGA fuel samples:

1. On samples in which there was no contact with the Inconel-600 sheath of the thermocouples, all samples survived the tests in excellent condition. Minor cracking occurred in all samples quenched from 800° and 1000°C.
2. For those samples in which the fuel was in contact with the Inconel-600 thermocouple sheath, no obvious reactions occurred up to 1000°C. Above approximately 1050°C, eutectics were formed of uranium with nickel, chromium and iron, and possibly zirconium with nickel and iron, which resulted in localized melting of the surfaces of the fuel samples.

These results indicate satisfactory behavior of TRIGA fuel for temperatures to at least 1200°C. Under conditions where the clad temperature can approach the fuel temperature for several minutes

TABLE 2-2
CHARACTERISTICS OF 45U-53Zr-1Er-1H SAMPLES BEFORE AND AFTER QUENCH TESTS

Drop Temp (°C)/ Sample No.	Before Drop			After Drop			Net Change		
	Weight (g)	o.d. (mm)	Length (mm)	Weight (g)	o.d. (mm)	Length (mm)	Weight (g)	o.d. (mm)	Length (mm)
800/1 ^(a,b)	19.9152	12.916	18.240	19.8002	12.883	18.164	-0.115	-0.033	-0.076
1000/2 ^(a,b)	15.9549	12.916	14.600	15.8835	12.725	14.364	-0.0714	-0.191	-0.236
1200/3 ^(b,c)	16.0684	12.913	14.628	15.6037	12.903	14.554	-0.3647	-0.010	-0.075
1150/4 ^(d,e,f)	16.7173	12.913	15.283	(g)	13.081 ^(h)	15.265	(g)	+0.168 ^(h)	-0.018 ^(h)
1050/5 ^(d,e,f)	19.4721	12.913	18.062	19.4988	12.883	17.290	+0.0267	-0.031	-0.142
1100/6 ^(d,f,i)	14.6627	12.916	13.536	14.4414	12.746	13.533	-0.2213	-0.170	-0.003
1100/7 ^(a,d,j)	19.1613	12.918	17.689	18.3849	12.845	17.424	-0.7764	-0.074	-0.264
1100/8 ^(d,f,i)	18.2588	12.916	16.855	17.5136	12.715	16.607	-0.7452	-0.201	-0.249
1200/9 ^(a,d,j)	13.9545	12.950	12.901	13.895	12.728	12.690	-0.0600	-0.208	-0.211

(a) Refers to samples actually quenched. Other samples shown were either intentionally, or because of alloying with the temperature-measuring thermocouple, not quenched but were heated to the indicated temperature, then cooled in the argon atmosphere of the experiment furnace.

(b) Tantalum susceptor.

(c) Sample reacted with thermocouple and tantalum susceptor.

(d) Molybdenum susceptor.

(e) Localized melting on all surfaces.

(f) No quench.

(g) Not weighed, thermocouple attached to sample by alloying.

(h) Dimensions over bumps of once-molten material.

(i) Measured temperature by inserting thermocouple.

(j) Molybdenum cup between thermocouple and fuel sample.

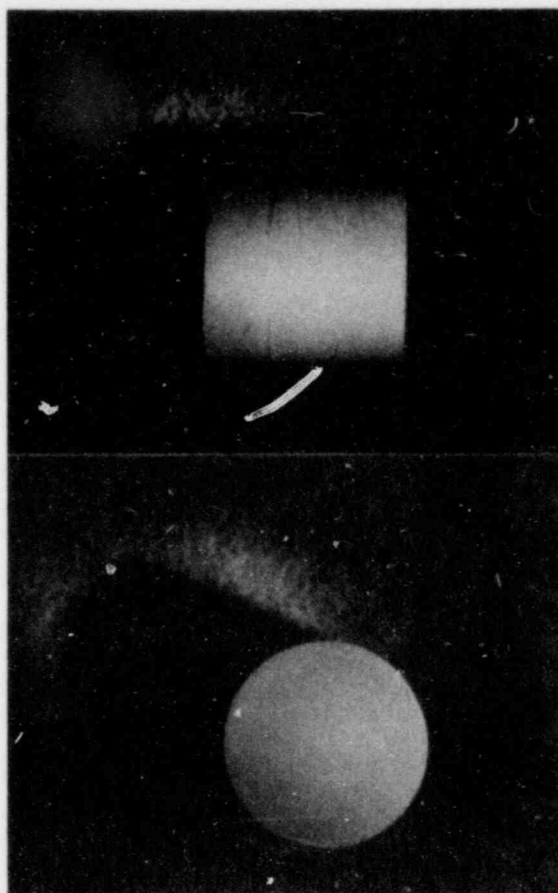


Fig. 2-19. Fuel sample 9 after quench from 1200°C

(which may allow formation of eutectics with the clad), the results indicate satisfactory behavior to about 1050°C. This is still about 50° to 100°C higher than the temperature at which internal hydrogen pressure is expected to rupture the clad, should the clad temperature approach that of the fuel. It should be pointed out that thermocouples have performed well in instrumented TRIGA fuel elements at temperatures up to 650°C in long-term steady-state operations, and up to 1150°C in very short time pulse tests.

2.13. IRRADIATION EFFECTS

Most of the irradiation experience to date is limited to the uranium-zirconium hydride fuels used in the SNAP and TRIGA reactors (normally containing about 8 to 10 wt % uranium). The presence of uranium influences the radiation effects because of the damage resulting from fission recoils and fission gases. Some significant conclusions may be drawn from the results of these experiments (Ref. 13). The uranium is present as a fine dispersal (about 1 μ m diam.) in the U-ZrH fuels, and hence the recoil damage is limited to small regions within the short (~ 10 - μ m) range of the fission recoils. Transmission electron microscope studies of irradiated samples indicated the presence of voids within the range of fission recoils, in the vicinity of the uranium fuel particles, with the regions far from the fuel particles retaining a microstructure similar to that of unirradiated material. The U-ZrH fuel exhibits high growth rate during initial operation, the so-called "offset" growth period, which has been ascribed to the vacancy-condensation type of growth phenomenon over the temperature range where voids are stable. The voids are also associated with the delta- and epsilon-phase banding. Banding indicates the presence of stress-related fuel growth phenomena, since the growth is highly radial-oriented. An important consideration in integrating the irradiation results is the presence of thermal gradients in the fuel samples in the tests. It is evident from the

SNAP data that the fuel in the reactor tests, and in capsule tests which closely simulated the SNAP reactor operating conditions and thermal gradients, showed a different temperature-swelling relationship compared with other capsule fuel experiments where the fuel temperatures were more uniform (Ref. 13).

The behavior of unfueled delta and epsilon zirconium hydride under fast neutron irradiation has also been investigated (Ref. 44). In these experiments, the samples (35 mm x 15 mm in diameter) were irradiated at temperatures up to 580°C to fluences up to 1.15×10^{25} n/m² ($E > 1$ MeV). The axial thermal gradients were between 520° and 230°C. The postirradiation tests included measurements of density and dimensions, metallography, x-ray diffraction, and hydrogen analysis. The results indicated that the epsilon phase had swelled about 0.51%, whereas the delta phase showed no growth. The growth was attributed to a radiation-induced change of the tetragonal epsilon structure, which leads to an increase of the axial ratio. The volume growth of two-phase (delta plus epsilon) specimens was found to be related directly to the epsilon content.

The GCFR fuel irradiation capsule F-3 irradiated in the EBR-II reactor contained specimens of $ZrH_{1.5}$ and $ZrH_{1.7}$. These samples were irradiated at about 400°C to much higher fluences than in any previous test, approximately 5 to 7×10^{26} n/m² ($E > 0.1$ MeV). The postirradiation examination indicates that no significant damage or swelling has occurred in the irradiated specimens.

The calculated core burnup characteristics* of TRIGA fuel with high enriched uranium (HEU) are as follows:

Metal % Burnup	70% Enriched (Present FLIP) ~3500 MW Days	93% Enriched 14 MW TRIGA ~7000 MW Days	14 MW TRIGA-LEU
Average	0.8 - 1.0%	1.7 - 2.0%	~1%
Peak**	1.25 - 1.45%	2.1 - 2.4%	~1.3%

NVT - to fuel and clad

	3500 MW Days	7000 MW Days
$\phi(>1 \text{ Mev})^{***}$	4.5×10^{21}	9.0×10^{21}
$\phi(<1 \text{ ev})$	3.0×10^{21}	6.0×10^{21}

The USAEC has set a limit of 2.54 mm (0.1 in.) for longitudinal growth of fuel elements for all TRIGA pulsing reactors. Nevertheless, fuel elements have operated intact for long periods in TRIGA reactors with cladding elongations of up to 36 mm (Yugoslavia, non-pulsing TRIGA). A mechanical ratcheting mechanism caused these unusual elongations, which can be eliminated by suitable fuel element design.

Burnups of up to approximately 0.52 total metal at. % (75% burnup of the U-235) have been attained successfully with TRIGA fuel elements. The results of extensive irradiation tests in the SNAP reactor program have led to empirical correlations between swelling under steady-state operation and the important variables of temperature, fuel

* Initial core, not an equilibrium burnup cycle value.

** Averaged over element with maximum power density and assuming no shuffling of fuel during core life. The portion of this element next to a water hole or flux trap will have increased burnup if not rotated or shuffled periodically. The U-235 constitutes 2.5 metal atom % in the 70% enriched fuel, 4.2 metal atom % in the 93% enriched fuel and 4.8 metal atom % of the 14 MW LEU fuel. These are the upper limits of burnup.

*** Add ~20% for ϕ 7.05 Mev.

composition, burnup, neutron flux and fluence (Ref. 3). The offset growth during early life (up to about 0.1 metal at. % burnup) is ascribed to the vacancy-condensation type growth phenomenon.

Instrumented pulsing fuel elements have been fabricated to determine the temperature distributions in the fuels and claddings and to record the gas pressures in the fuel elements.

In the ACPR fuel elements a small gas gap (375 μm , 0.015 in) is provided by means of dimples in the cladding which introduces a thermal resistance to control heat flow rates from the fuel immediately after pulsed operation and prevent film boiling (Ref. 3). The fuel elements can be pulsed to temperatures greater than 1150°C without exceeding the safe level of the internal hydrogen pressure. Test elements with hot spots of about 1175°C have exhibited local swelling after about 200 to 400 pulses. The swelling resulted from internal porosity formed by the gradual nucleation, growth, and migration of hydrogen bubbles toward the surface in the hot spot region.

In standard, nongapped, TRIGA fuel, the steady-state power temperature levels increase after pulsing and the increases are attributed to the formation of a gas gap between the fuel and cladding. The gap formation is caused by the rapid fuel expansion during the pulse heating of the fuel.

An in-pile, high-temperature King furnace (Ref. 59) provides a means to investigate the behavior of reactor fuels in high-temperature transients (e.g., HTGR coated fuel particles) under transient heating conditions by neutron pulsing to over 3000°C.

Much information on irradiation effects on hydride fuels has been generated in the SNAP-reactor program (Ref. 13). The swelling of

the U-Zr hydride fuels at high burnups is governed by three basic mechanisms:

1. The accommodation of solid fission products resulting from fission of U-235. This led to an early estimated growth of approximately 1.2% to 2.3% $\Delta V/V$ per metal at. % burnup. This mechanism is relatively temperature insensitive.
2. The agglomeration of fission gases at elevated temperatures (above 1300°F). This takes place by diffusion of the xenon and krypton to form gas bubbles.
3. A saturable cavity nucleation phenomenon which results from the nucleation and growth of irradiation-formed vacancies into voids over a certain range of temperatures where the voids are stable. The saturation of growth by this mechanism was termed offset swelling. It was deduced from the rapid decrease in fuel-to-cladding ΔT experienced during the early part of the irradiation. The saturation was reached in approximately 1500 hr.

The highest swelling occurs in the beta-phase at elevated temperatures by means of the fission gas agglomeration because the low creep strength of the beta-phase cannot accommodate the fission gas pressures in the gas bubbles. Sweeping of fission gases may occur by phase boundary motion if the beta phase forms in the irradiated fuel (Ref. 13). For example, beta-phase fuel specimens (H/Zr - 1.2 and 1.4) were post-irradiation annealed after low-temperature 700°F irradiation. Annealing for 211 hr at 1300°F produced small amounts of shrinkage, whereas annealing for 75 hr at 1600°F produced 15% to 25% swelling. Annealing delta-phase fuel (H/Zr - 1.6 to 1.9) under the same conditions produced small amounts of shrinkage or swelling - less than 1.5% in all cases (Ref. 45). The shrinkage of the fuel upon post-irradiation annealing

is ascribed to recovery of the matrix from damage caused at temperatures lower than those employed during annealing. Anomalous shrinkage may also be attributed to hydrogen loss.

The samples exhibiting large decreases in density showed cracks and voids which suggest fission gas agglomeration (Ref. 45). The void clusters in high-hydride samples were correlated with epsilon-phase banding and led to the conclusion that some damage mechanism (other than fission gas agglomeration) takes place based on an apparent delta-epsilon phase boundary damage phenomenon (Ref. 46). The epsilon-phase irradiation data indicate the presence of stress-related fuel growth phenomena since the growth is highly radial oriented (Ref. 47). An important consideration in integrating the irradiation results is the presence of thermal gradients in the fuel samples in the tests. It is evident from the data that the fuel in the reactor tests, and in capsule tests which closely simulated the SNAP reactor operating conditions and thermal gradients, showed a different temperature-swelling relationship compared to the other capsule fuel experiments where the fuel temperatures were more uniform (Ref. 47).

A number of attempts has been made to correlate the measured swelling of SNAP-reactor fuels with burnup, temperature, and hydrogen content. Large uncertainties in each of these parameters have made it necessary to use a statistical sample (Ref. 48) based on clusters of points rather than on individual datum points.

The observed dimensional changes indicate variations in the ratio of volumetric change to diameter change large enough to establish the importance of diameter as an engineering variable (Ref. 48). The fuel growth is isotropic only when the ratio $\Delta V/V$ to $\Delta D/D$ is 3. The fuel growth is preferred in the radial direction when the ratio is between 2 and 3, and in the axial direction when the ratio is greater than 3. Axial shrinkage gives rise to a ratio of less than 2. The mean value of the ratio for the delta-phase is 2.8 ± 0.4 , and for the epsilon-phase is about 1.6 ± 0.5 .

In the swelling correlations used for the SNAP-reactor fuels, the bulk average temperature is considered to be identical to the arithmetic average of the peak centerline temperature and the surface temperature (Ref. 47). The time-variation of this temperature was calculated from the beginning-of-life (BOL) temperature, based on the cladding thermocouple readings, the measured end-of-life (EOL) fuel $\Delta D/D$, and the following fuel swelling model (Ref. 47):

$$\Delta V/V = 3B + \exp (-K/T) \quad ,$$

where B = burnup in metal at. %,

K = constant ($\sim 30,000$), and

T = bulk average fuel temperature (in degrees R).

As stated earlier, the greatest success has been achieved by using the offset, or equilibrium, bulk average fuel temperature which the fuel reaches after offset swelling has been completed (Ref. 49). The fuel swelling observed in the SNAP S8ER and S8DR reactor experiments was generally lower than predicted from the capsule tests, except for the NAA-121 capsule test in which the temperature profiles were similar, and the data correlate well with the S8DR data (Ref. 47) (Table 2-3 and Figs. 2-20 through 2-24).

A model of swelling based on burnup and temperature led to the relationship for volumetric growth of (Ref 49):

$$\% \frac{\Delta V}{V} = \alpha B + \beta \exp (-\lambda/T) \quad ,$$

$$\text{where } \% \frac{\Delta V}{V} = 2 \frac{\Delta D}{D} + \frac{\Delta L}{L} \quad ,$$

B = Burnup in metal at. %,

T = bulk average fuel temperature, and

α , β , and λ are constants.

TABLE 2-3^(a)
SELECTED DATA FROM CAPSULE IRRADIATION TESTS

NAA Test	U-content (Weight %)	H/Zr	Burnup (Met. at. %)	Temperature (°F)	Time (Hr)	Swelling (% $\Delta V/V$) (% $\Delta D/D$)	
-43	10	1.0	2.05	768	9,652	7.1	--
"	"	"	1.89	---	9,652	7.1	--
"	"	"	3.35	730	13,370	7.3	--
-53	"	1.77	0.68	1300	2,076	1.3	--
"	"	"	1.03	1213	3,876	4.5	--
"	"	"	0.36	1515	1,385	2.7	--
-115-1	"	1.69	0.42	1550-1600	---	1.65	--
"	"	1.63	0.41	1560-1610	---	4.01	--
-116-1	"	1.6 to 1.9	0.15	<700	---	1.60	0.59
-116-2	"	"	0.65	<700	---	3.45	--
-116-1	19	1.76	0.29	500	---	1.56	0.59
-116-1	19	1.75	0.29	500	---	2.56	0.97
-117-1	10	1.55 1.35	0.77	1492	---	5.06	--
"	"	1.69 1.62	0.77	1496	---	2.85	--
"	"	1.69 1.53	0.77	1539	---	2.82	--
"	"	1.60 1.61	0.31	1511	---	1.06	--
"	"	1.70 1.44	0.31	1449	---	0.91	--
"	"	1.85 1.62	0.37	1287	---	1.07	--
-75	15% U + 6.5 % H _f	1.44 1.23	1.05	1075	5,253	3.77	--
"	"	1.45 1.48	2.15	1011	5,253	7.11	--
"	"	1.41 1.33	0.5	1059	2,955	4.94	--
"	"	1.40 1.52	1.26	914	2,955	4.11	--

(a) Taken from Ref. 13.

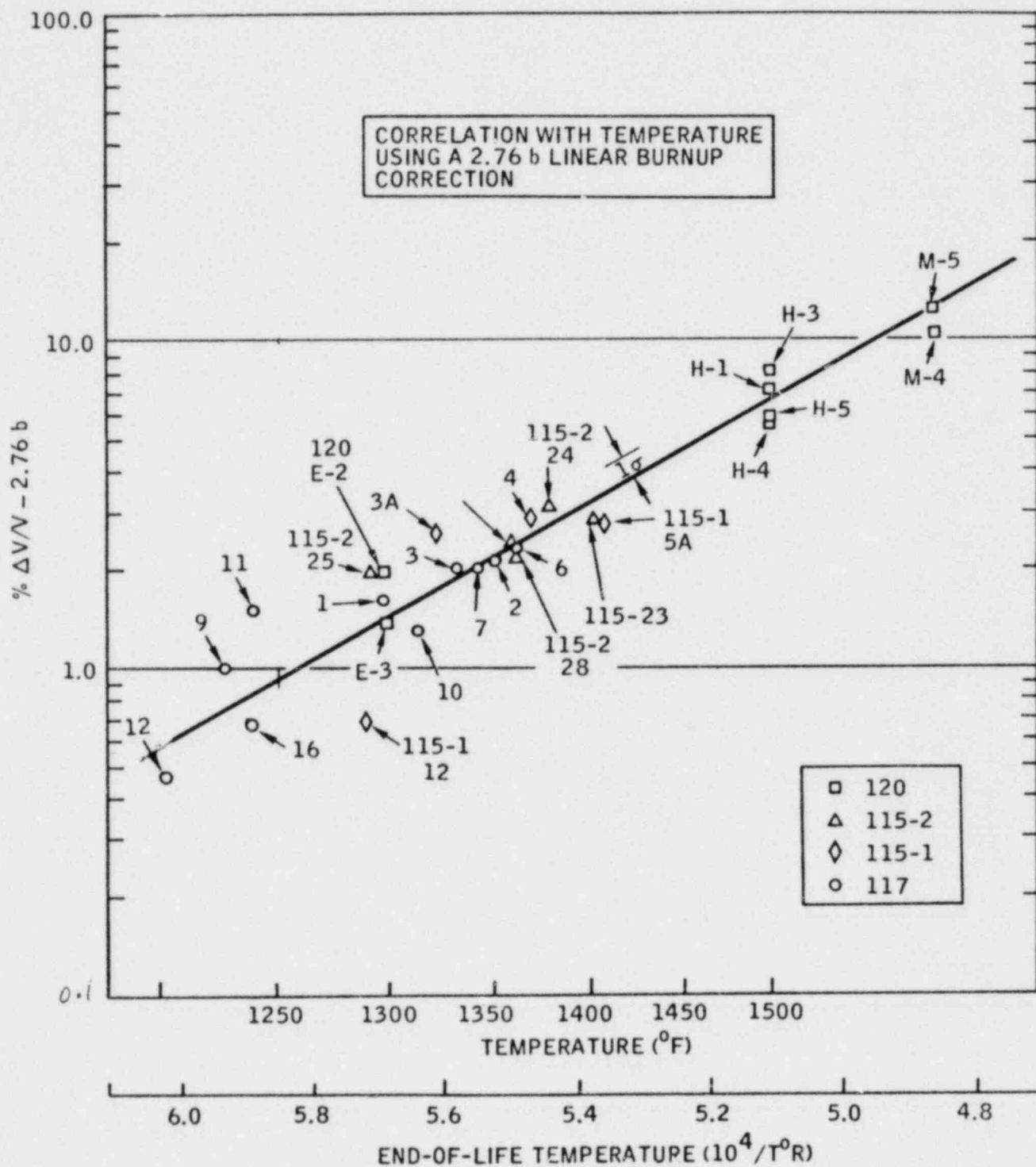


Fig. 2-20. Zirconium hydride fuel swelling (from Ref. 58)

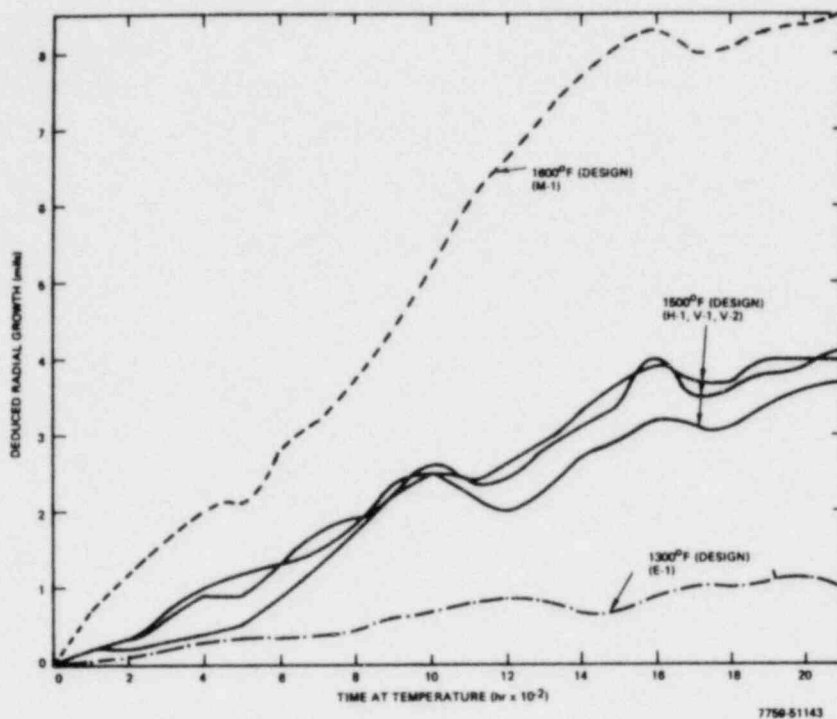
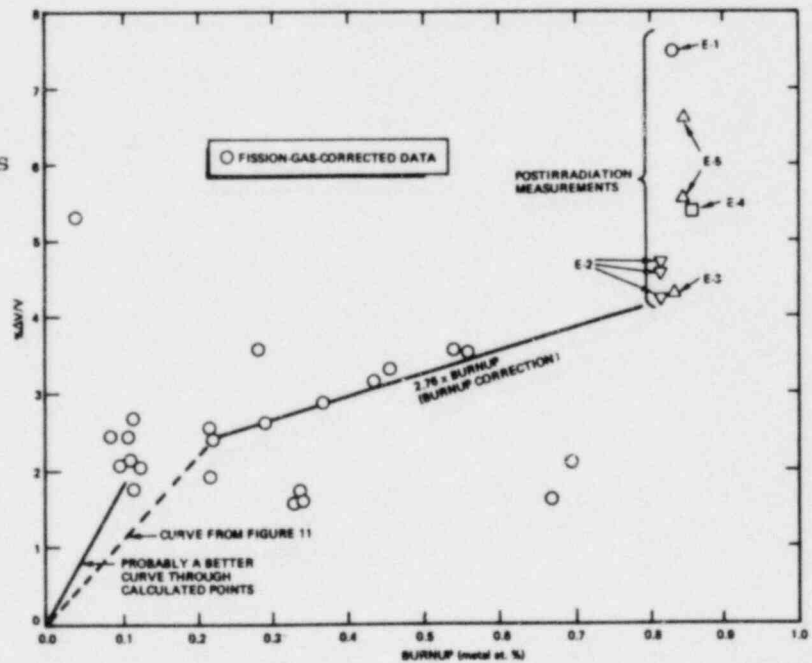


Fig. 2-21. Radial fuel growth vs time (based on fuel-cladding ΔT) (from Ref. 58)

Fig. 2-22. Volume increase vs burnup for the 1300°F subcapsules (based on fuel-cladding ΔT) (from Ref. 58)



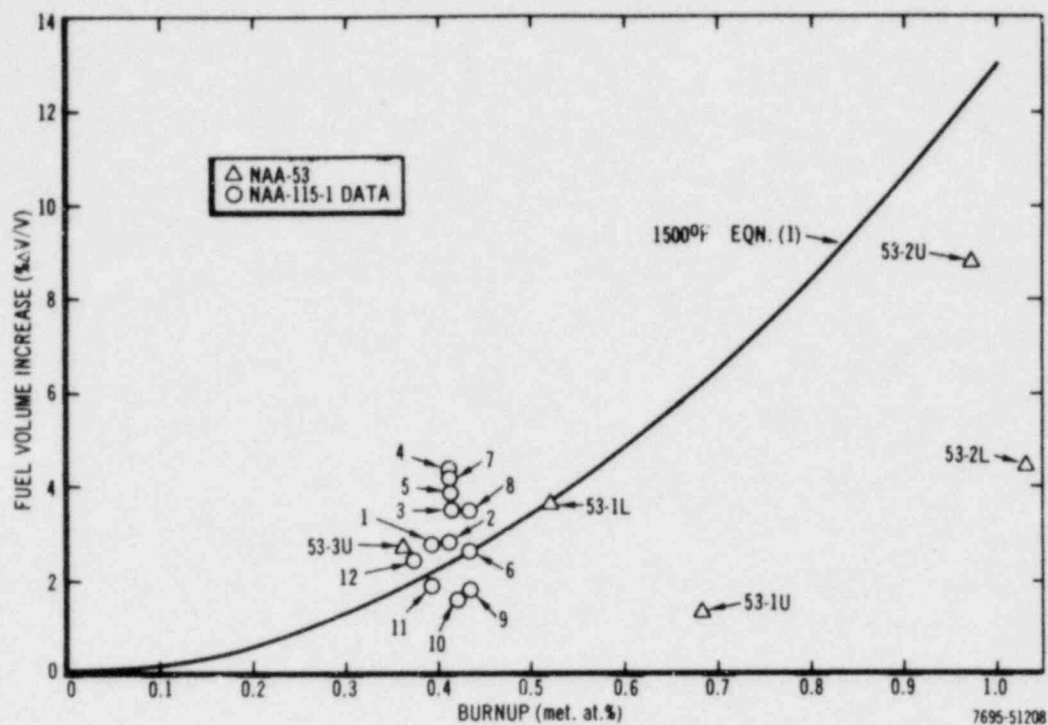


Fig. 2-23. Fuel growth vs burnup with NAA-53, NAA-115-1, and empirical correlations (from Ref. 58)

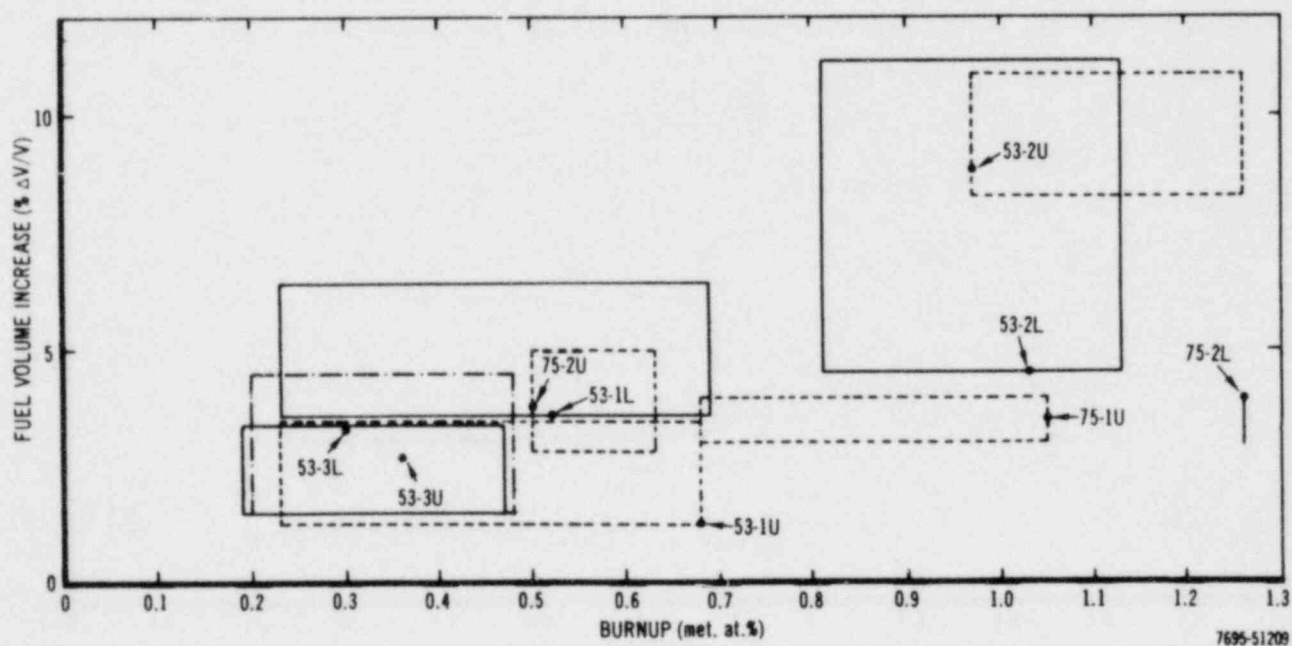


Fig. 2-24. Fuel growth vs burnup with NAA-53 and NAA-75 data (from Ref. 58)

The fuel swelling data are usually plotted as log (corrected volume growth) versus $1/T$. The corrected volume growth for offset swelling has been given variously by:

$\frac{\Delta V}{V} - 2.76 B$, $\frac{\Delta V}{V} - 2.8 B$, and more recently $\frac{\Delta V}{V} - 3 B$ (the Bonzer-Swenson correlation).

The S8DR data tend to show a greater temperature sensitivity than that shown by the Bonzer-Swenson correlation, but the bulk of the data does fall within the Bonzer-Swenson scatter band and indicates a higher temperature sensitivity only if considered as a separate data set (Ref. 13). The S8DR data show a correlation of $(\frac{\Delta V}{V} - 3 B)$ of 0.8% at 1250°F, 0.4% at 1200°F, and 0.2% at 1150°F. The total correlation is as follows:

$$\left(\frac{\Delta V}{V} - 3B \right) = 5.5 \exp \left(- \left\{ 2.3 \overset{\circ}{b} \exp \left[\frac{21.5}{2} \left(\frac{1860}{T} - 1 \right) \right] + 21.5 \left(\frac{1860}{T} - 1 \right) \right\} \right),$$

where

b = burnup, metal at. %,

$\overset{\circ}{b}$ = burnup rate, burnup/10,000 hr operation, and

T - absolute operating temperature of fuel at time offset fuel growth has been completed, °R.

3. PULSE HEATING

The U-ZrH fuel elements used in the TRIGA reactor are capable of operation under conditions of transient experiments for delivery of high-intensity bursts of neutrons. For these experiments, the reactor is equipped with a special control rod mechanism that provides a method of obtaining a step reactivity change of predetermined magnitude in the reactor. During the nuclear pulse, nearly all the energy is stored as thermal energy in the fuel material. This results in an almost instantaneous rise in the temperature of the fuel body. Fuel elements with 8.5 wt % U have operated repeatedly in the Advanced TRIGA Prototype Reactor (ATPR) to peak power levels of over 8,000 MW providing a neutron fluence per pulse of about 10^{15} nvt.

The ATPR fuel elements have been subjected to thousands of pulses of 2,000 MW and more. The nuclear safety stems from the large prompt negative temperature coefficient of reactivity of the uranium-zirconium hydride fuel-moderator material. The inherent prompt shutdown mechanism of TRIGA reactors has been demonstrated extensively during the tens of thousands of pulses conducted on TRIGA reactors. These tests involved step insertions of reactivity of up to 3-1/2% $\delta k/k$. An in-pile test has been performed on fuel elements of a modified design (gapped) for high performance in the TRIGA Annular Core Pulse Reactor (ACPR). As expected, there was satisfactory fuel body performance after 400 pulses at temperatures up to the design point of 1000°C (Ref. 3). There was no evidence of interaction between the clad and the fuel. The transient gas pressure in the space between the fuel and the clad was measured during the pulse, and peak pressures were found to be less than 40 psia - well below the upper bound implied by the equilibrium pressure data. As testing at higher temperatures continued,

there was some evidence that at hot-spot regions, where the temperature near the fuel surface reached about 1200°C, the fuel gradually swelled slightly over a large number of pulses under the influence of the hydrogen pressure in small bubbles that nucleated in the hot spots ($\sim 1200^\circ\text{C}$, $\text{U-ZrH}_{1.65-1.70}$) and formed a gray patch.

The basic cause of fuel body distress after more than 200 pulses appears to be local overheating of the fuel body as a result of thermal-neutron flux peaking in a water-cooling channel adjacent to the fully enriched special test elements. The mechanism by which this apparently occurs is as follows: if the internal temperature and hydrogen concentrations are sufficient to produce bubbles of hydrogen gas, plastic or creep yielding of the fuel material over successive pulses may permit an increase in bubble size over a period of time; this would tend to increase the disruptive force while weakening the restraining matrix, thus gradually producing the porous expanded fuel which constitutes the gray patch. Other possible mechanisms were considered but have been tentatively rejected on the basis of evidence obtained in the postexperiment analyses.

There was no indication that excessive heat-transfer rates contributed to cladding distortion. Cladding material cut from the fuel elements appeared to be straight and true. When the initial longitudinal cut was made, the cladding sprang open slightly to a uniform gap of about 3/16 in., as would be expected from the residual stress remaining due to the action of the die in the final drawing operation during fabrication. The thermal-stress distortion due to excess heat flux would have tended to produce residual stress in the opposite direction. Additionally, the external surface discoloration was far less than for a normal element, after either normal maximum steady-state or pulsed operation.

Internal gas pressure was indicated to be negligible compared with the yield point for the cladding. The pressure-transducer calibration was re-checked and found satisfactory after the test. In addition, a pressure-instrumented element (identified as 2E) was pressurized to 50 psi after the test and maintained pressure overnight, which verified that there was no measurable leak in the element. It should be noted that gas chromatography was performed for gas extracted from element 2E. In this test no hydrogen gas was detected, although the instrument has a high sensitivity for hydrogen.

The mechanisms of nucleation, growth, and migration of gas bubbles in solids have been studied extensively in recent years, mainly in connection with fission-gas formation and swelling in nuclear reactor fuels and helium formation by nuclear transmutation in alloys. This information is most useful in elucidating the damage mechanism. Barnes (Ref. 50), Nichols (Ref. 51), and Lawton (Ref. 52) have presented reviews of this subject. The conclusions reached from the results of recent studies can be summarized as follows: The behavior of the gas bubbles determines how much gas is released and how much swelling is produced by the gas retained. The bubbles can migrate bodily under the influence of various driving forces and by various mechanisms. In most cases the bubbles migrate in a direction determined by temperature gradients, stress gradients, and moving dislocation lines or grain boundaries. Analysis indicates that small bubbles are dominated by the behavior of dislocation lines; however, as their size increases the temperature gradient becomes more important. Models based on the behavior of dislocation lines and grain boundaries are appropriate when the temperature gradients are small; little gas escapes and swelling is then the main consequence.

On the other hand, it has been found that where steep temperature gradients occur, the behavior is more complex, different models being required for each temperature zone. At high temperatures the gradient

can drag bubbles from dislocations, and the bubbles migrate up the temperature gradients, becoming trapped on grain boundaries where gas is released periodically. Barnes (Ref. 50) has postulated that bubbles migrate predominantly by a surface diffusion mechanism, while the main parameters determining the behavior of the bubbles are temperature gradient, bubble radius, surface diffusion, vapor pressure of the solid, and surface tension. If the material is stressed, the moving dislocations will drag the bubbles. The temperature gradient largely determines the critical sizes of the bubbles.

These observations are in line with the conclusions of the present authors regarding the mechanism of formation of the distressed area in the hot spots in the pulsed special test fuel. This area evidently was subjected to a temperature range and to cycles of thermal gradients and stress gradients such as to favor the nucleation, migration, and growth of hydrogen bubbles toward the surface.

As the bubbles grew in size, the internal hydrogen pressure could not be accommodated by the fuel matrix, which consequently gradually yielded and swelled until it made contact with the cladding. With subsequent pulses the cladding itself is compelled to make provision for fuel swelling by its own expansion (Ref. 52). That is, the cladding will be deformed by swelling of the fuel body at temperatures below those where creep or hydrogen gas pressure can cause the cladding to expand. This phenomenon follows from the fact that in a pulse, the rapidly heated fuel expands thermally more than the cladding and thereby forces the cladding to expand once the initial gap has been bridged by swelling of the fuel body. This accounts rather well for the fact that the changes are governed by a progressive process and do not take place during a few pulses.

From the results of these tests, it can be concluded that U-ZrH fuel elements can be safely pulsed even to very high fuel temperatures. Not until after more than 400 pulses to fuel temperatures

in excess of 1100°C did measurements show that two of the five test elements exceeded the conservative dimensional tolerances. In the first 200 pulses, there was no external evidence of change in any of the five special test elements. The practical consequences of this are several-fold. First, small power reactors using U-ZrH fuel can safely sustain accidental power excursions to high fuel temperature. Second, and perhaps more significant, high-level pulsing reactors (fluences of 10^{15} nvt) can be operated with U-ZrH fuel with a reasonable fuel lifetime. For example, the annular core TRIGA reactor at JAERI (Japan) has operated since 1975, with over 1000 pulses of all sizes at fuel temperatures of up to 1000°C. Further, with regard to standard types of TRIGA research reactors, it is evident that present peak fuel temperatures are conservative.

The results of rapid dehydriding tests indicate that the endothermic nature of hydrogen loss slows down the rate of temperature rise. When the hydride specimens are rapidly heated to elevated temperatures in a dynamic vacuum system, large scale internal cracking takes place, whereas when a backpressure of hydrogen is maintained (as in a clad fuel element) the hydride fuel body contains relatively small bubbles which are associated with the grain structure and substructure of the material.

In the SNAPTRAN (Ref. 53), TREAT (Ref. 54), and KIWI-TNT (Ref. 55) tests, high-hydride modified U-Zr hydrides have been pulse heated to destruction. In these specimens the hydrogen content (1.82 wt %) was very high and the temperatures were high enough to rupture or granulate the fuel. In the KIWI-TNT transient tests the specimens were exposed to a large nuclear transient under the following conditions (Ref. 55):

1. In containers designed to withstand internal pressures of 140,000 psi.

2. In chambers sealed with prestressed rupture disks calibrated to burst within 5% of specific pressure values.
3. In a container in which the hydrogen gas released from the fuel acted on a free piston which impacted a copper anvil and produced an indentation that was calibrated to give a measure of the gas pressure as a function of time.

In type 3 tests, extensive cracking of the fuel took place since large void space was available. Much less fracture occurred in type 1 and type 2 tests since the internal gas pressure was balanced. In some of the TREAT tests, the fuel irradiation temperatures were high enough to melt the fuel (about 1800°C).

ERBIUM ADDITIONS

All available evidence indicates that the addition of erbium to the U-ZrH introduces no deleterious effects to the fuel. Erbium has a high boiling point and a relatively low vapor pressure so that it can be melted into the uranium-zirconium uniformly. The erbium is incorporated into the fuel during the melting process. All the analyses that have been made on the alloy show that the erbium is dispersed uniformly, much as is the uranium. Erbium is a metal and forms a metallic solution with the uranium-zirconium; thus there is no reason to believe that there will be any segregation of the erbium. Erbium forms a stable hydride (as stable as zirconium hydride) which also indicates that the erbium will remain uniformly dispersed through the alloy. Also, since neutron capture in erbium is an $n-\gamma$ reaction, there are no recoil products.

The erbium cannot migrate or segregate in the fuel at the temperatures and times involved since the diffusion rates are much too low. Intermetallic diffusion rates follow an exponential relationship with

temperature and are extremely low at the operating temperatures for this type of alloy. Thus, with a conservative diffusion coefficient of 10^{-13} cm²/sec at 800°C, the diffusion distance would be about 0.1 mm/yr. Hence there could not be any significant migration during the lifetime of the fuel.

4. LIMITING DESIGN BASIS PARAMETER AND VALUES

Fuel-moderator temperature is the basic limit of TRIGA reactor operation. This limit stems from the out-gassing of hydrogen from the ZrH_x and the subsequent stress produced in the fuel element clad material. The strength of the clad as a function of temperature can set the upper limit on the fuel temperature. A fuel temperature safety limit of 1150°C for pulsing, stainless steel U- $\text{ZrH}_{1.65}$ or Er-U- $\text{ZrH}_{1.65}$ fuel is used as a design value to preclude the loss of clad integrity when the clad temperature is below 500°C . When clad temperatures can equal the fuel temperature, the fuel temperature limit is 950°C . There is also a steady-state operational fuel temperature design limit of 750°C based on consideration of irradiation- and fission-product-induced fuel growth and deformation. This is a time and temperature-dependent fuel growth as discussed earlier. A maximum temperature of 750°C has been used as the operational design basis temperature because resulting average fuel temperatures result in insignificant calculated fuel growth from temperature-dependent irradiation effects. (For ACPR fuel, where burnup is extremely low, the steady-state operational fuel temperature design criterion is 800°C).

The dissociation pressure of the zirconium-hydrogen system is the principal contributor to the fuel element internal pressure at fuel temperatures above $\sim 800^\circ\text{C}$. Below $\sim 800^\circ\text{C}$ trapped air and fission product gases can be the major contributors to the internal pressure. At equilibrium condition, this pressure is a strong function not only of temperature but also the ratio of hydrogen to zirconium atoms and the carbon content of the material. The current upper limit for the hydrogen-to-zirconium ratio is 1.65; the design value is 1.6. The carbon content is currently about 0.2% (2000 ppm). The equilibrium hydrogen

pressure as a function of temperature for the fuel is shown in Fig. 2-9. Figure 4-1 shows the temperature dependent strength curves currently used for stainless steel in TRIGA design work.

For the ACPR fuel, optimized for pulsing with a built-in thermal barrier (0.01 in. gap) between the fuel and clad, the clad temperature does not exceed 280°F (138°C). At 280°F (138°C) the yield strength of type 304L stainless steel is 38,000 psi and the ultimate strength is 68,000 psi. The stress imposed on the clad S by the internal pressure is

$$S = \frac{r_c}{t_c} P_h \quad , \quad (1)$$

where

r_c = the clad radius

t_c = the clad thickness (in the same units as r_c)

P_h = the hydrogen pressure.

For the dimensions of the clad, the maximum allowable hydrogen pressure is

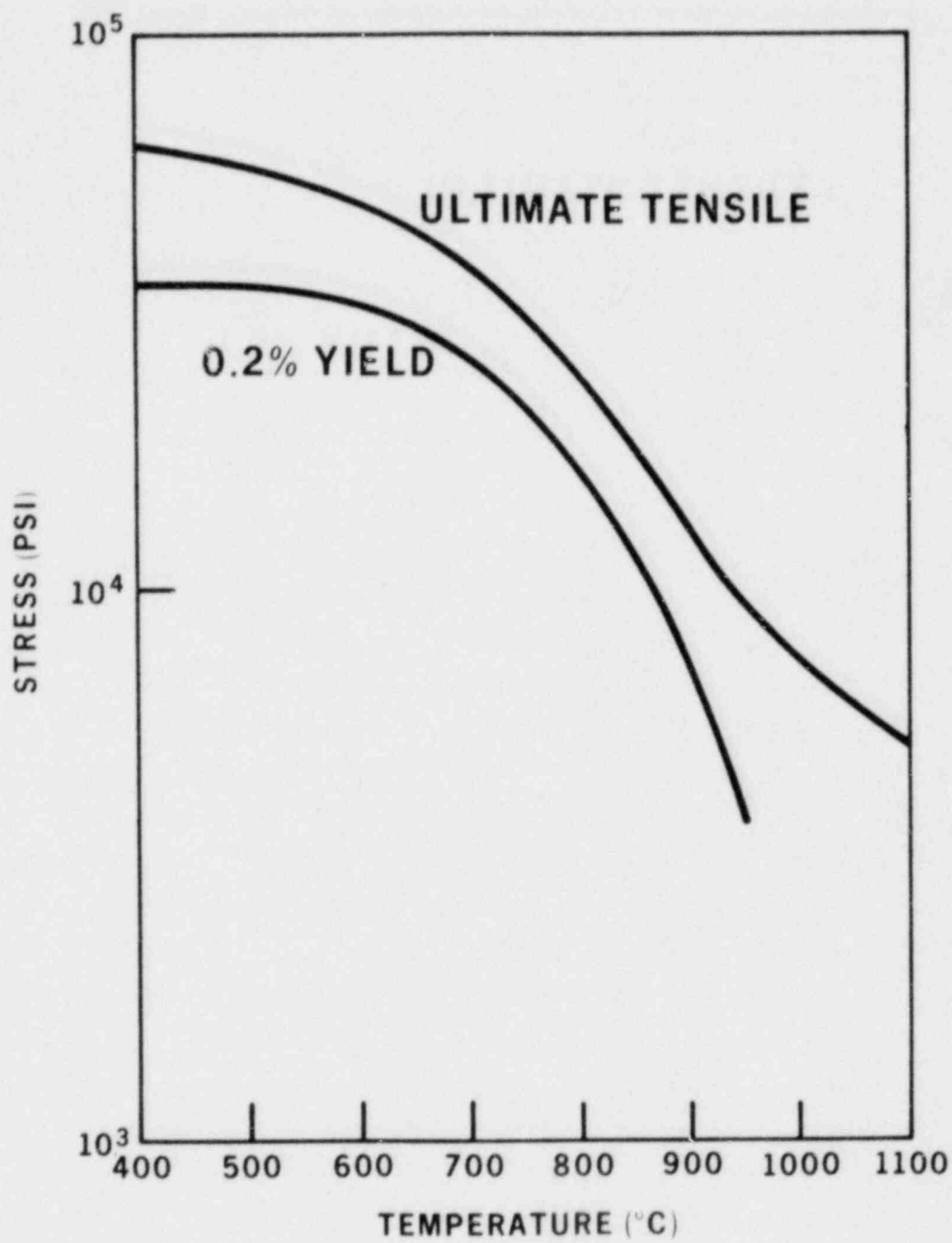
$$P_h = \frac{38,000}{0.739/0.020} = 1025 \text{ psi} \quad (2)$$

to produce yield, and

$$P_h = \frac{68,000}{0.739/0.020} = 1840 \text{ psi} \quad (3)$$

to rupture the clad. From Fig. 2-9 it can be seen that for U-ZrH_{1.65} the fuel temperatures that will produce these pressures, under equilibrium conditions, are 1080°C and 1140°C.

The equilibrium condition defined above never occurs, however, because the fuel is not at a constant temperature over the whole volume.

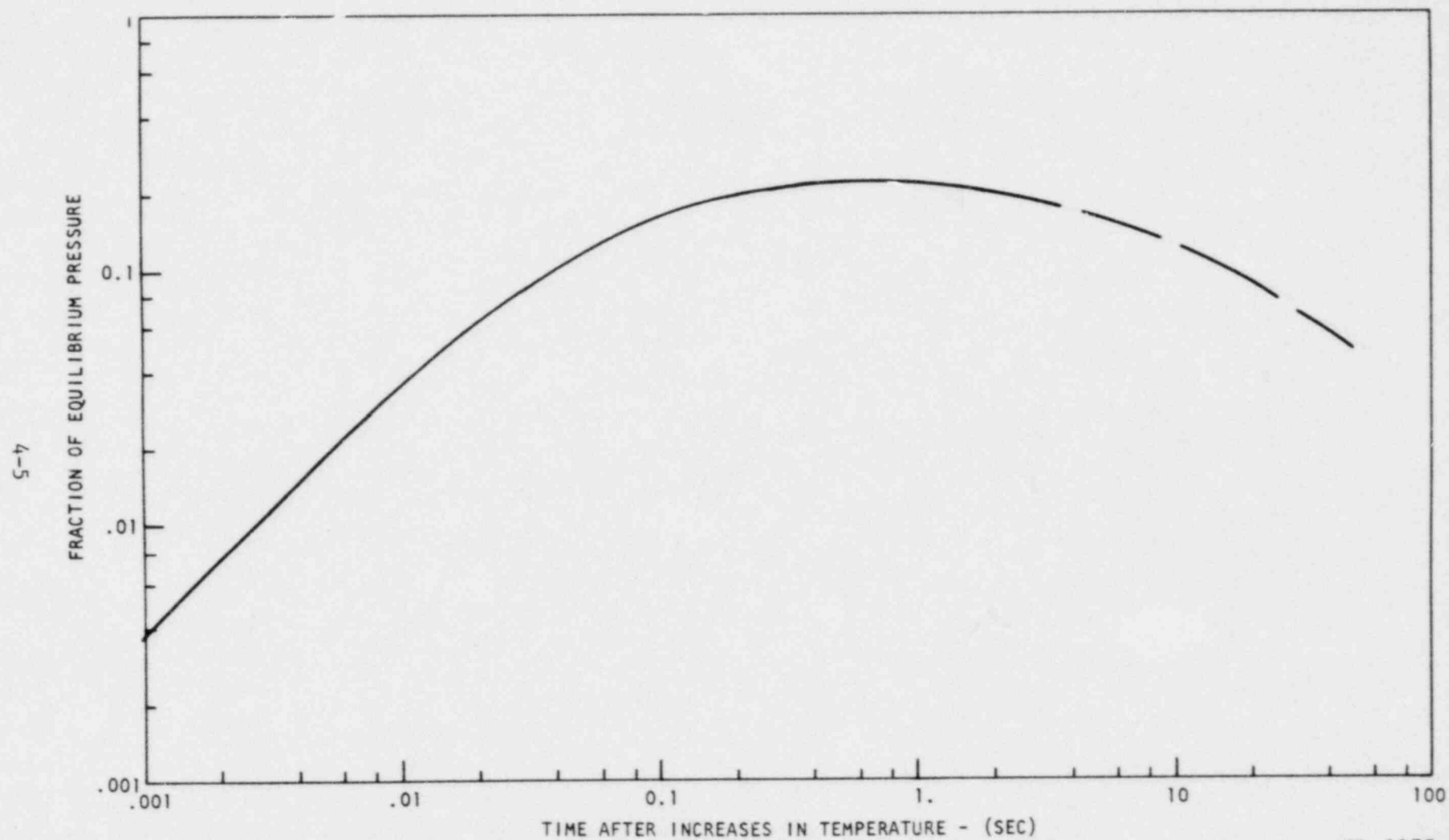


EL-1617

Fig. 4-1. Strength of type 304 stainless steel as a function of temperature

Consequently the hydrogen pressures will be much lower than the equilibrium values calculated for the maximum temperature. As hydrogen is released from the hot fuel regions it is taken up in the cooler regions and the equilibrium that is obtained is characteristic of some temperature lower than the maximum. To evaluate this reduced pressure, diffusion theory is used to calculate the rate at which hydrogen is evolved and reabsorbed at the fuel surface. In the closed system considered here, not only does the hydrogen diffuse into the fuel/fuel clad gap, but it diffuses back into the fuel in the regions of lower fuel temperature. When the diffusion rates are equal, an equilibrium condition will exist.

In Fig. 4-2 the ratio of the fuel element internal pressure to the equilibrium hydrogen pressure is plotted as a function of time after a step increase in temperature. The maximum fuel temperature is 1150°C for which the equilibrium hydrogen pressure in $\text{ZrH}_{1.65}$ is 2080 psi. The calculation indicates, however, that the internal pressure increases for about 0.3 sec at which time the pressure is ~ 420 psi, or $\sim 20\%$ of the equilibrium value. After this time, the pressure slowly decreases as the hydrogen continues to be redistributed along the length of the element from the hot regions to the cooler regions. Calculations were also made for step increases in power to the peak fuel temperatures of 1200°C and 1350°C . Over this range the time to the peak pressure and the fraction of the equilibrium pressure value achieved were approximately the same as for the 1150°C case. Thus, if the clad remains below $\sim 138^{\circ}\text{C}$, the maximum internal pressure that would produce the yield stress in the clad is 1025 psi (see Eq. 2) and the corresponding equilibrium hydrogen pressure could be five times greater or ~ 5000 psi. This pressure corresponds to a maximum fuel temperature of $\sim 1240^{\circ}\text{C}$ in $\text{ZrH}_{1.65}$. Similarly, the equilibrium hydrogen pressure could be 5×1840 or 9200 psi before the ultimate clad strength was reached corresponding to a fuel temperature of $\sim 1300^{\circ}\text{C}$.



EL-1175

Fig. 4-2. Fuel element internal pressure versus time after a step increase in maximum fuel temperature (from Ref. 10)

The ultimate strength of the clad decreases slowly to about 57,000 psi at 500°C. Since the pressure is a strong function of fuel temperature, the fuel temperature to produce rupture decreases very slowly over this range, remaining at 1300°C for a clad temperature up to 300°C and decreasing to ~1293°C and 1282°C for clad temperatures of 400°C and 500°C respectively. For non-gapped TRIGA pulsing fuel elements, the clad temperature during heat flow from a pulse is greater than the 138°C ACPR value but normally <500°C.

Measurements of hydrogen pressure in TRIGA fuel elements during steady-state operation have not been made. However, measurements have been made during transient operations and compared with the results of an analysis similar to that described here.

These measurements indicated that in a pulse in which the maximum temperature in the fuel was greater than 1000°C, the maximum pressure was only ~6% of the equilibrium value evaluated at the peak temperature. Calculations of the pressure resulting from such a pulse using the methods described above gave calculated pressure values about three times greater than the measured values.

An instantaneous increase in fuel temperature will produce the most severe pressure conditions. When a peak fuel temperature of 1150°C is reached by increasing the power over a finite period of time, the resulting pressure will be no greater than that for the step change in power analyzed above. As the temperature rise times become long compared with the diffusion time of hydrogen, the pressure will become increasingly less than for the case of a step change in power. The reason for this is that the pressure in the clad element results from the hot fuel dehydriding faster than the cooler fuel rehydrides (takes up the excess hydrogen to reach an equilibrium with the hydrogen over-pressure in the can). The slower the rise to peak temperature, the lower the pressure because of the additional time available for rehydriding.

The foregoing analysis gives a strong indication that the clad will not be ruptured if fuel temperatures are never greater than in the range of 1240° to 1300°C, providing the clad temperature is less than 500°C. However, a conservative safety limit of 1150°C has been chosen for this condition. As a result, at this safety limit temperature the pressure is at least a factor of 5 (and up to a factor of 18) lower than would be necessary for clad failure. A factor of 5 is more than adequate to account for uncertainties in clad strength and manufacturing tolerances. The integrity of the clad has been demonstrated by TRIGA reactor pulse experiments to fuel temperatures $\geq 1150^{\circ}\text{C}$.

Under any condition in which the clad temperature increases above 500°C, such as during a loss-of-coolant accident or under film boiling conditions, the temperature safety limit must be decreased as the clad material loses much of its strength at elevated temperatures. To establish this limit it is assumed that the fuel and the clad are at the same temperature. An analysis for this condition indicates that at a fuel and clad temperature of $\sim 950^{\circ}\text{C}$ the equilibrium hydrogen pressure produces a stress on the clad equal to its ultimate strength. There are no conceivable circumstances that could give rise to a situation in which the clad temperature was higher than the fuel.

The same argument about the redistribution of the hydrogen within the fuel presented earlier is valid for this case also. In addition, at elevated temperatures the clad becomes permeable to hydrogen. Thus, not only will hydrogen redistribute itself within the fuel to reduce the pressure but some hydrogen will escape from the system entirely.

The use of the ultimate strength of the clad material in the establishment of the safety limit under these conditions is justified because of the transient nature of such accidents.

5. FISSION PRODUCT RETENTION

A number of experiments have been performed to determine the extent to which fission products are retained by U-ZrH fuel. Experiments on fuel with 8.5 wt % U were conducted over a period of 11 years and under a variety of conditions. Results prove that only a small fraction of the fission products are released, even in completely unclad U-ZrH fuel. The release fraction varies from 1.5×10^{-5} for an irradiation temperature of 350°C to $\sim 10^{-2}$ at 800°C (Ref. 56). The experiments on fission product release include:

1. 1960 - The measurement of the quantity of a single fission product isotope released from a full-size TRIGA element during irradiation.
2. 1966 - The measurement of the fractional release of several isotopes from small specimens of TRIGA fuel material during and after irradiation at temperatures ranging from $\sim 25^\circ\text{C}$ to 1100°C .
3. 1971 - The measurement of the quantities of several fission product isotopes released from a full-size TRIGA fuel element during irradiation in a duplication of the 1960 experiment.

Post-irradiation annealing measurements of the release from small fuel samples heated to 400°C .

Post-irradiation annealing release measurements from a small previously-irradiated fuel sample which had experienced fuel burnup to $\sim 5.5\%$ of the U-235.

4. SNAP - Measurements made as part of the Space Nuclear
Auxiliary Power reactor program.

The experiments show that there are two mechanisms involved in the release of fission products from TRIGA fuel, each of which predominates over a different temperature range. The first mechanism is that of fission fragment recoil into the gap between the fuel and clad. This effect predominates in fuel at temperatures up to $\sim 400^{\circ}\text{C}$; the recoil release rate is dependent on the fuel surface-to-volume ratio but is independent of fuel temperature. Above $\sim 400^{\circ}\text{C}$, the controlling mechanism for fission product release from TRIGA fuel is a diffusion-like process, and the amount released is dependent on the fuel temperature, the fuel surface-to-volume ratio, the time of irradiation, and the isotope half-life.

The results of the TRIGA experiments, and measurements by others of fission product release from SNAP fuel, have been compared and found to be in good agreement.

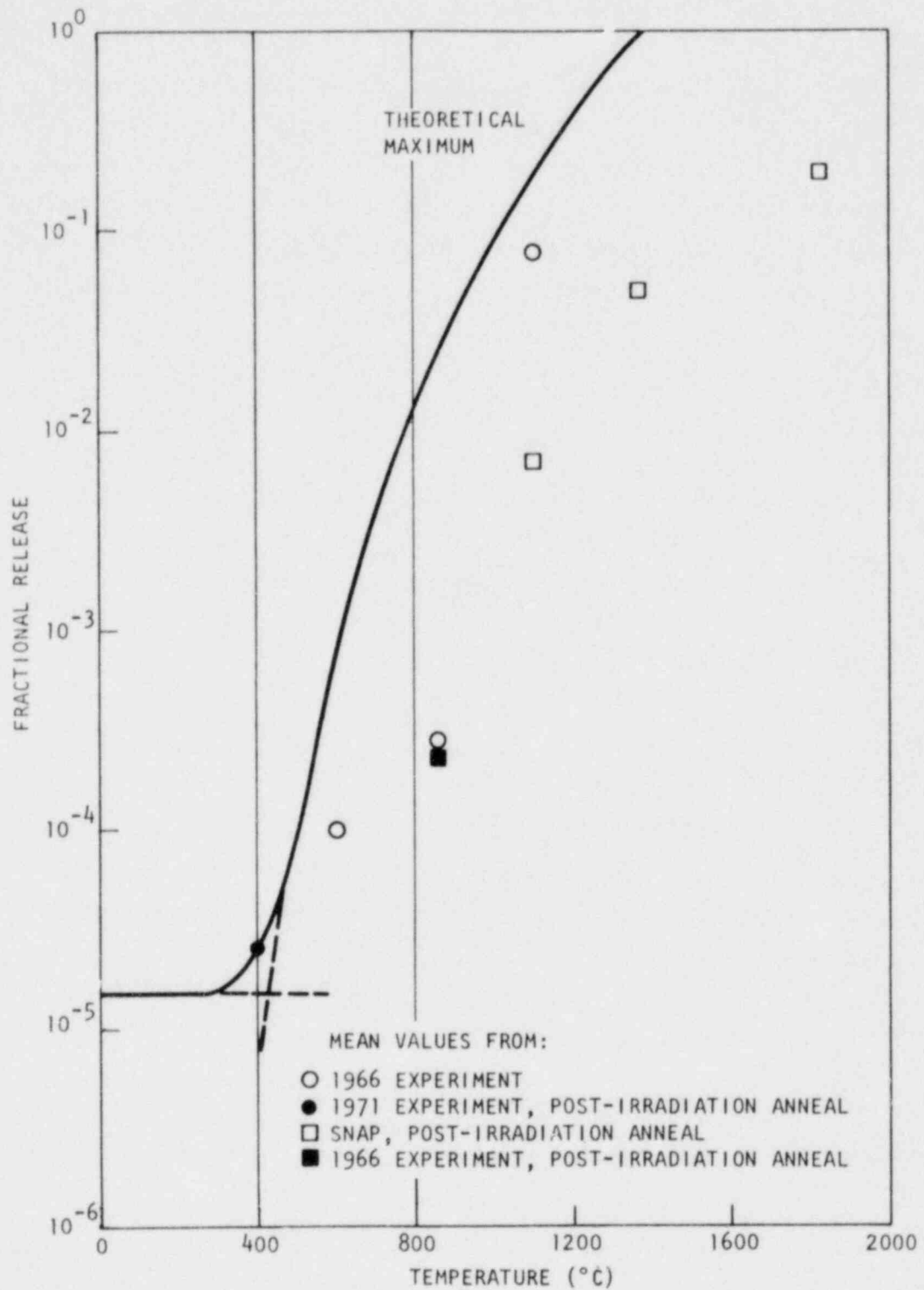
The fractional release, ϕ , of fission product gases into the gap between fuel and clad from a full-size standard TRIGA fuel element is given by:

$$\phi = 1.5 \times 10^{-5} + 3.6 \times 10^3 e^{-1.34 \times 10^4 / (T + 273)} ,$$

where T = fuel temperature, $^{\circ}\text{C}$.

This function is plotted in Fig. 5-1. The first term of this function is a constant for low-temperature release; the second term is the high-temperature portion.

The release fractions have all been normalized to a standard ratio of fuel-clad gap to fuel diameter, although individual measurements were made with different geometry.



75LC373

EL-1615

Fig. 5-1. Fractional release of gaseous fission products from TRIGA fuel showing theoretical maximum, and experimental values above 400°C corrected to infinite irradiation (from Ref. 10)

The curve in Fig. 5-1 applies to a fuel element which has been irradiated for a time sufficiently long that all fission product activity is at equilibrium and the release fraction is at its theoretical maximum. Figure 5-1 shows that the measured values of fractional releases fall well below the curve. Therefore, for safety considerations, this curve gives very conservative values for the high-temperature release from TRIGA fuel.

Also worthy of note are the following conclusions from the TRIGA fission product release experiments:

1. Because the samples were unclad, the high-temperature measurements were made on essentially dehydrided U-Zr. Post-irradiation annealing measurements indicate that the dehydriding process did not significantly affect the release rate.
2. Part of the 1971 experiments was the measurement of the release from a post-irradiation anneal of a sample of fuel that had been irradiated to a burnup of $\sim 5.5\%$ of the U-235 (or 1.1% of the total uranium atoms). The results of this part of the experiment indicated that the effects of long-term irradiation of the fuel on fission product release are small, at least for total burnup equivalent of the maximum that has been achieved.
3. The release fraction for accident conditions is characteristic of the normal operating temperature, not the temperature during accident conditions. This is because the fission products released as a result of a fuel clad failure are those that have collected in the fuel-clad gap during normal operation.

4. Since the fuel temperature distribution is not isothermal, it is necessary to integrate the temperature-dependent release fraction over the temperature distribution in a fuel element.

The results of recent studies (Ref. 57) in the TRIGA reactor at General Atomic on fission product release from fuel elements with high uranium loadings (up to 45 wt % U) agree well with data just presented from similar experiments with lower U loadings. As was the case with the lower U loadings, the release was determined to be predominantly recoil controlled at temperatures $\leq 400^{\circ}\text{C}$ and controlled by a migration or diffusion-like process above 400°C . Low temperature release appears to be independent of uranium loadings but the high temperature release seems to decrease with increasing weight fractions of uranium. The correlation used to calculate the release of fission products from TRIGA fuel remains applicable for the high uranium loaded (TRIGA-LEU) fuels as well as the 8.5 w/o U-ZrH fuel for which it was originally derived. This correlation predicts higher fission product releases than measurements would indicate up to 1100°C . At normal TRIGA operating temperatures ($<750^{\circ}\text{C}$) there is a safety factor of approximately four between predicted and experimentally deduced values.

The LEU fuel data in general show consistent, although somewhat higher release ($\leq 1.5 \times 10^{-5}$, however) than found in the earlier studies, up to 400°C . In contrast, the values at 1100°C show substantial variation even for fuel samples of the same composition. An example is an order of magnitude difference in release between two 30 w/o samples. The 45 w/o samples show a similar behavior. However, the data at 1100°C were all found to be the same or less than the release obtained for the 8.5 w/o samples studied earlier. A sample of reference 8.5 w/o uranium containing fuel was tested along with the higher weight percent samples. The results confirm the early 8.5 w/o data.

Efforts to determine the cause for the large observed variations for the higher weight percent samples at higher temperatures consisted of both metallographic and microprobe examination of the same fuel samples used in the fission gas release tests. Table 5-1 describes the results of these tests. It is apparent from the metallographic examination, shown in column 5 of Table 5-1, that the visual variations between samples do not correspond to the observed increases in fission gas release. All four samples studied show some degree of characteristic dendritic structure. However, no obvious correlation could be made between the fission gas release values shown in column 4 of Table 5-1 and observable structural difference using metallographic techniques. Microprobe examination did however reveal substantial differences, as shown in Fig. 5-2. Figure 5-2 contains photographs of x-ray maps for uranium distribution in the fuel samples studied. The pictures show the relative uranium concentration near a zirconium hydride dendrite. The dendrite appears as the cross shaped void in each of the photographs. The photographs are all 100x magnifications of the samples studied. The highest releasing sample, containing 8.5 w/o uranium, was found to have a relatively uniform dispersal of uranium throughout the matrix (uranium particle size <1 micron). On the other hand, uranium was found to concentrate at the ZrH dendrite boundaries as the uranium content was increased. This is evident in the distribution photographs shown in Fig. 5-2A (8.5 w/o), 5-2B (30 w/o) and 5-2D (45 w/o). The uranium segregation and concentration at the boundaries appears to increase with increasing weight percent uranium (concentration thicknesses of up to ~5 microns).

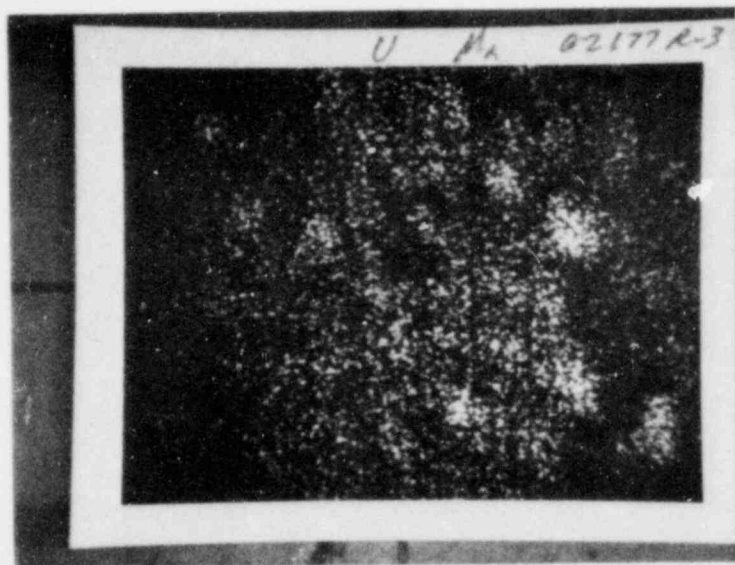
Comparing Figs. 5-2C and 5-2D one can also see an obvious difference between the uranium concentration at the boundaries in samples of the same composition. The pictures were taken of two samples containing 45 w/o uranium but manufactured at different times. The sample in Fig. 5-2D was enriched to 20% with U-235 whereas that in Fig. 5-2C was made from natural uranium. The uranium appears to be less

TABLE 5-1
SUMMARY OF METALLOGRAPHIC AND MICROPROBE EXAMINATION

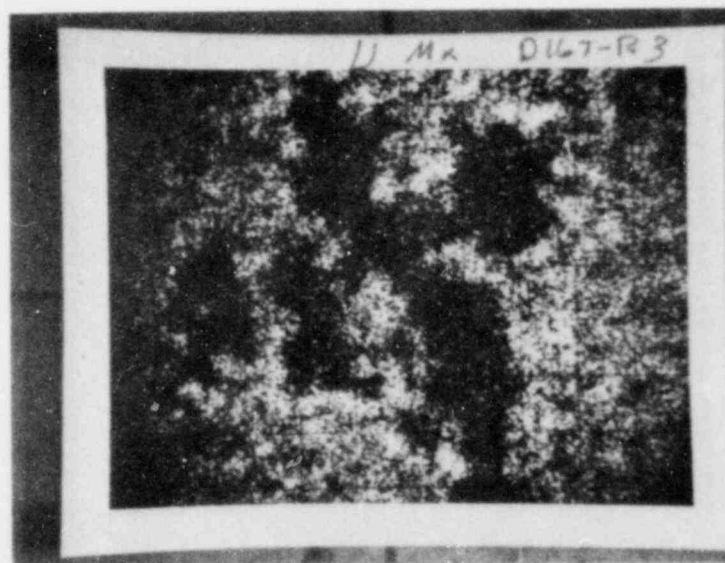
Sample	Number	Weight % Uranium	% Enrichment	Kr-85m R/B(a) @ 1100°C	Metallographic Appearance		Microprobe Uranium Distribution
					Grain Size	Dendrite Size	
62177	R-3	8.5	20	1.12×10^{-1}	Large	Large	Diffuse
D167	R-3	30	0	6.40×10^{-2}	Small	Small	Slight Segregation
D168	R-1	45	0	1.20×10^{-2}	Small	Large	Segregated
E451	R-1	45	20	4.18×10^{-4}	Small	Large	Highly Segregated

(a) R/B = ratio of fission gas release rate to birth rate in the fuel
(uncorrected for container or cladding effects).

A



B



C



D

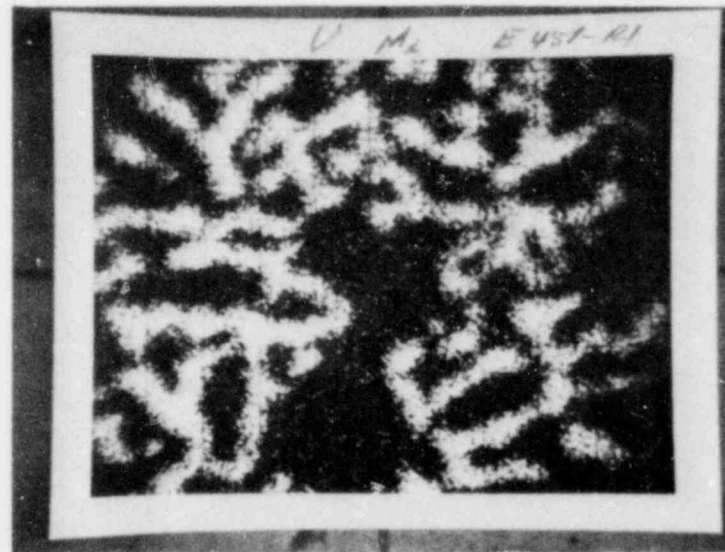


Fig. 5-2. Photographs of Uranium X-ray Distribution Maps in TRIGA Fuel Specimens.
 (A) 8.5 w/o-20% enriched, (B) 30 w/o, (C) 45 w/o and (D) 45 w/o-20% enriched

EL-3479

concentrated in Fig. 5-2C which also gave a much higher fission gas release value (factor of 30 higher) than did the sample represented in Fig. 5-2D. Thus, the microprobe examination of the fuel samples revealed micro-segregation of uranium in fuel containing higher uranium loading. Because of the higher localized concentration of uranium as the maximum weight fraction increases, it is postulated that the fission gas release is lowered at high temperature as a result of trapping of the recoiled fragments in the uranium. In the low weight percent samples the uranium is finely dispersed so that a fission fragment born in the uranium will have a high probability of recoiling out of the uranium particle into the ZrH matrix through which it will diffuse. As the uranium particles increase in size, with higher loadings, the probability of recoiling out of the uranium particle decreases and fewer fragments are deposited in the ZrH. It was also found that the particle size or degree of microsegregation of uranium varied widely for a given uranium loading, making it apparent that some physical parameter such as temperature, (possibly sample heating and cooling rates during manufacture) must also be involved in the segregation phenomenon.

This change in the uranium atom distribution does not affect the low temperature release as the probability that a fission fragment will be born within a recoil range of the surface is unchanged. Thus, the fission gas release at high temperature (1100°C) was found to decrease with increasing uranium content and remain essentially unchanged at temperatures below 400°C.

6. THERMAL CYCLING TESTS

A most encouraging feature of the results of the thermal cycling tests (Ref. 57) is the excellent physical stability exhibited by the 45 wt % - 20% enriched fuel rods. The thermal cycle tests were performed over the temperature range of 500° to 725°C. The specimens were subjected to 100 thermal cycles out-of-pile and then cycled 32 times in a neutron flux of $\sim 4 \times 10^{12}$ n/cm²-sec in the King furnace in the GA TRIGA reactor. There were no significant changes in dimensions in the out-of-pile tests, and a small decrease in weight was measured. The in-pile cycling test showed a small decrease in both length and diameter, which may be related to a loss of hydrogen during this test. In these thermal cycling tests the specimens traversed a phase transformation temperature of the uranium (orthorhombic to tetragonal at 653°C). The structure consisting of a fine dispersion of the uranium in a still largely (~ 85 v/o) zirconium hydride matrix precludes anisotropic growth from taking place as a result of cycling through the phase transformation temperature, since the hydride matrix restrains the uranium particles and accommodates the transformation stresses and strains. The data on the thermal cycling tests are listed in Table 6-1.

The results of the microprobe studies indicate that the uranium in the 45 wt % U samples is uniformly distributed on a macroscale, but it has segregated in the inter-dendritic regions of the cast structure. This leads to a relatively coarser grain size than in the 8.5 wt % samples, but the uranium is still in the form of a dendritic, broken up structure surrounded by the hydride matrix. Such a structure would be expected to exhibit the dimensional stability that was observed in the thermal cycling tests. It also leads to the type of fission product release described in the earlier section. Examples of the electron microprobe distribution maps in the TRIGA fuel specimens are shown in Fig. 5-2.

TABLE 6-1
RESULTS OF THERMAL CYCLING TESTS

No. of Cycles	Length (cm)			Diameter (cm)				Weight (gms)	Irrad. Unirrad.
	L-1	L-2	Avg.	D-1	D-2	D-3	Avg.		
0	5.089	5.091	5.090	1.285	1.288	1.288	1.287	58.114	Unirrad.
25	5.089	5.093	5.091	1.289	1.288	1.288	1.288	58.114	Unirrad.
50	5.088	5.092	5.090	1.289	1.289	1.289	1.289	58.111	Unirrad.
75	5.088	5.092	5.090	1.289	1.291	1.290	1.290	58.109	Unirrad.
100	5.088	5.091	5.089	1.290	1.289	1.290	1.290	58.108	Unirrad.
116	5.078	5.080	5.079	1.291	1.285	1.275	1.283	57.997	Irrad.
132	5.064	5.068	5.066	1.285	1.278	1.280	1.281	57.875 ^(a)	Irrad.

(a) Represents 0.4% loss in weight.

7. ACKNOWLEDGMENTS

The author would like to thank Gordon West, Fabian Foushee, and A. J. Gietzen for their review of this paper.

8. REFERENCES

1. Wallace, W. P., M. T. Simnad, and B. Turovlin, "Fabrication and Properties of U-Zr Hydride Fuel Elements for TRIGA Reactors," Nucl. Metallurgy, 5, 49, (1958).
2. Simnad, M. T., G. Hopkins, and J. Shoptaugh, "Fuel Elements for the TRIGA Mark III Pulsing Reactor," Trans. Am. Nucl. Soc., 7:110 (1964).
3. Simnad, M. T., and J. B. Dee, "Equilibrium Dissociation Pressures and Performance of Pulsed U-ZrH Fuels at Elevated Temperatures," Proc. Symp. Thermodynamics of Nuclear Materials, Vienna, Austria, IAEA, 1967.
4. Simnad, M. T., and R. Chesworth, "TRIGA Research Reactor Experimental Instrumentation," Proc. Symp. Research Reactor Instrumentation, Tehran, Iran, IAEA, 1972.
5. Whittemore, W. L., et al., "Stability of U-ZrH_{1.7} TRIGA Fuel Subjected to Large Reactivity Insertions," GA Report GA-6874, General Atomic Company, 1965.
6. Whittemore, W. L., et al., "Characteristics of Large Reactivity Insertions in a High Performance TRIGA Core," GA Report GA-6216, General Atomic Company, 1965.
7. Hasenkamp, F. A., "Measured Performance of the Annular Core Pulse Reactor," Trans. Am. Nucl. Soc., 11:284 (1968).
8. Simnad, M. T., "Study of FLIP Fuels for TRIGA Reactors," GA Report Gulf-GA-A9910, General Atomic Company, 1970.
9. West, G. B., and J. Shoptaugh, "Experimental Results from Tests of 18 TRIGA-FLIP Fuel Elements in the Torrey Pines Mark F Reactor," GA Report GA-9350, General Atomic Company, 1969.
10. Simnad, M. T., F. Foushee, and G. West, "Fuel Elements for Pulsed TRIGA Research Reactors," Nucl. Tech., 28, 31-56 (Jan. 1976).

11. Lundy, T. S., and E. E. Gross, "An Evaluation of Solid Moderating Materials," USAEC Report ORNL-2891, Oak Ridge National Laboratory, April 1960.
12. Mueller, W. M., et al., Metal Hydrides, Academic Press, New York, 1968.
13. Lillie, A. F., et al., "Zirconium Hydride Fuel Element Performance Characteristics," USAEC Report AI-AEC-13084, Atomics International, June 19, 1973.
14. Harde, R., and K. W. Stoeher, "A Sodium-Cooled Power Reactor Experiment Employing Zirconium-Hydride Moderator," in Third Geneva Conference Proceedings, United Nations, Geneva, v. 6, p. 353 (P/537), 1965.
15. Vasil'ev, G. A., et al., "Space Energy Distribution of Reactor Neutrons in Metal Hydrides," Vopr. Fiz. Zashch. Reaktorov 5, 91 (1972).
16. Andriyevskii, R. A., et al., "Properties and Behavior of Moderator Materials under Irradiation," in Fourth Geneva Conference Proceedings, United Nations, Geneva, v. 10, p. 383 (P/452), 1971.
17. Vetrano, J. B., "Hydrides as Neutron Moderator and Reflector Materials," Nucl. Eng. Des. 14, 390 (1970).
18. Gylfe, J. D., et al., "Evaluation of Zirconium Hydride as Moderator in Integral Boiling Water-Superheat Reactors," USAEC Report NAA-SR-5943, North American Aviation, 1962.
19. Moore, K. E., and M. M. Nakata, "Phase Relationships in Alpha-plus-Delta Region of the Zr-H System," USAEC Report AI-AEC-12703, Atomics International, September 30, 1968.
20. Moore, K. E., and W. A. Young, "Phase Relationships at High Hydrogen Content in SNAP Fuel System," USAEC Report NAA-SR-12587, Atomics International, 1968.
21. Raymond, J. W., and D. T. Shoop, "The Metallography of Zirconium-Base Alloy Hydrides," USAEC Report NAA-SR-Memo-10927, North American Aviation, 1965.
22. Mackay, K. M., Hydrogen Compounds of the Metallic Elements, F. N. Spoon, Ltd., London, 1966.

23. Raymond, J. W., "Equilibrium Dissociation Pressures of the Delta and Epsilon Phases in the Zirconium-Hydrogen System," USAEC Report NAA-SR-9374, North American Aviation, 1964.
24. Johnson, H. E., "Hydrogen Dissociation Pressures of Modified SNAP Fuel," AI-Rept. NAA-SR-9295, Atomics International, 1964.
25. Singleton, J. H., R. Ruke, and E. A. Gulbrensen, "The Reaction of Hydrogen with a 50 Weight Per Cent Alloy of Uranium and Zirconium Between 542°C and 798°C," Westinghouse Research Laboratories Report AECU-3630, November 16, 1956.
26. LaGrange, L. D., et al., "A Study of the Zirconium-Hydrogen and the Zirconium-Uranium-Hydrogen Systems Between 600°C and 800°C," J. Phys. Chem. 63, 2035 (1959), and General Atomic Laboratory Note Books.
27. Krause, H. H., H. E. Bigony, and J. R. Doig, Jr., "Phase Studies in the Zirconium-Hydrogen-Uranium System," Advances in Chemistry Series 39 Naustochiometric Compounds A.C.S. (Symposium) Washington, D.C., 1963.
28. Merten, U., and J. Bokros, "Thermal Migration of Hydrogen in Zirconium-Uranium-Hydrogen Alloys," J. Nucl. Mat. 10, 3, 201-08 (1963).
29. Paetz, P. and K. Lücke, "On the Kinetics of Hydrogen Engassing of Delta-Zirconium Hydride," Z. Metallkunde, 62(9), 657 (1971).
30. Meyer, R. D., and J. G. LeBlanc, "Negative Thermal Expansion in UZrH Reactor Fuel," Trans. Am. Nucl. Soc. 13, 2 (1970).
31. Leadon, B. M., et al., "Aerospace Nuclear Safety - SNAP, Part 5: Measurements and Calculations of Hydrogen Loss from Hydrided U-ZrH Fuel Elements During Transient Heating to Temperatures Near the Melting Point," Trans. Am. Nucl. Soc. 8, 547 (1965).
32. Taylor, R. E., "Pulse Heating of Modified Zr-H," USAEC Report NAA-SR-7736, North American Aviation, 1962.
33. Bernath, L. (ed), "SNAP-4 Summary Report," USAEC Report NAA-SR-8590, Atomics International, 1963.
34. Young, W. A., et al., "Thermophysical Properties of Unirradiated SNAP Fuels," USAEC Report NAA-SR-12607, Atomics International, 1968.
35. Beck, R. L., "Thermophysical Properties of Zirconium Hydride," Trans. Am. Soc. Metals 55, 556 (1962).

36. Foushee, F. C., "Physical Properties of TRIGA-LEU Fuel," GA Document E-117-834, February 1980.
37. Douglas, T. B., "The ZrH System: Some Thermodynamic Properties From a Heat Content Study," J. Am. Chem. Soc. 80, 5043 (1958).
38. Douglas, T. B., and A. C. Victor, "Heat Content of Zirconium and of Five Compositions of Zirconium Hydride from 0° to 900°C," Research Paper 2878, J. Res. Nat. Bur. Std. 61, 13 (1958).
39. Douglas, T. B., "High-Temperature Thermodynamic Functions for Zirconium and Unsaturated Zirconium Hydrides," J. Res. Nat. Bur. Std. 67A, 403 (1963).
40. Byron, G. F. (ed.), "SNAP Technology Handbook, Vol II: Hydride Fuels and Claddings," USAEC Report NAA-SR-8617, Atomics International, 1964.
41. Bokros, J. C., "Creep Properties of a U-ZrH Alloy," J. Nucl. Mater. 3, 216 (1961).
42. Berling, J. T., and G. D. Johnson, "Elevated Temperature Tensile Creep Properties of U-ZrH Alloy Hydrides," USAEC Report NAA-SR-11649, Atomics International, 1965.
43. Lindgren, J. R., and M. T. Simnad, "Low-Enriched TRIGA Fuel Water-Quench Safety Tests," Trans. Amer. Nucl. Soc., 33, 276 (Nov. 1979).
44. Paetz, P., "Neutron Irradiation Effects on Zirconium Hydride," J. Nucl. Mater. 43, 13 (1972).
45. Krupp, W. E., "Post-Irradiation Annealing of SNAP Fuel Irradiated at Low Temperatures - NAA-116 Experiment," USAEC Report NAA-SR-12089, Atomics International, 1967.
46. Forrester, R. E., and W. J. Roberts, "In-Pile Behavior of SNAP-8 Experimental Reactor Type Sublength Fuel Elements (NAA-115-2 Experiment)," USAEC Report NAA-SR-12625, Atomics International, 1968.
47. LeBlanc, J. C., "Prototype S8DR Fuel Element Performance Test (NAA-121-1 Experiment)," USAEC Report AI-AEC-13002, Atomics International, 1971.
48. Birney, K. R., "An Empirical Study of SNAP Reactor Fuel Irradiation Behavior," USAEC Report NAA-SR-12284, Atomics International, 1967.

49. Davies, N. F., and R. E. Forrester, "Effects of Irradiation on Hydrided Zirconium-Uranium Alloy, NAA-120-4 Experiment," USAEC Report AI-AEC-12963, Atomics International, 1970.
50. Barnes, R. S., and R. S. Nelson, "Theories of Swelling and Gas Retention in Reactor Materials," UKAEA Report AERE-R-4952 (1965).
51. Nichols, F. A., "Behavior of Gaseous Fission Products in Oxide Fuel Elements," USAEC Report WAPD-TM-570, Westinghouse Atomic Power Division, 1966.
52. Lawton, H., et al., "The Irradiation Behavior of Plutonium-bearing Ceramic Fuel," Symp. Fast Breeder Reactors, British Nuclear Energy Society, London, 1966.
53. Kessler, W. E., et al., "Zirconium-Hydride Fuel Behavior in the SNAPTRAN Transient Tests," Trans Am. Nucl. Soc. 9, 1, 155 (1966).
54. Miller, K. J., "Post-Irradiation Examination of Treat Capsule No. 5 through No. 9," USAEC Report NAA-SR-Memo-11374, North American Aviation, 1965.
55. Leadon, B. M., et al., "Aerospace Nuclear Safety--SNAP, Part 5: Measurements and Calculations of Hydrogen Loss from Hydrided Zirconium-Uranium Fuel Elements during Transient Heating to Temperatures Near the Melting Point," Trans. Am. Nucl. Soc. 8, 2, 547-8 (1965).
56. Foushee, F. C., and R. H. Peters, "Summary of TRIGA Fuel Fission Product Release Experiments," GA Report Gulf EES-A10801, Vol. II, General Atomic Company, and also S. Langer and N. L. Baldwin, "Fission Product Release Experiments on Uranium-Zirconium Hydride Fuels," GA Report Gulf GA-A10781, Vol. I, General Atomic Company, 1971.
57. Baldwin, N. L., F. C. Foushee, and J. S. Greenwood, "Fission Product Release from TRIGA Reactor Fuels," GA document E117-830, General Atomic Company, January 1980.
58. Simnad, M. T., "Review of UZr-Hydride Driver Fuel Elements for Thermionic Reactors," GA Report Gulf-GA-A11075, General Atomic Company, June 1972.
59. Anderson, E. E., et al., "An In-Core Furnace for the High-Temperature Irradiation Testing of Reactor Fuels," Nucl. Tech. 11:259 (1971).

APPENDIX

U.K. Plan 5 Prominent Scientists A-Exhibits

And changes were being made almost every hour.



TM

GENERAL ATOMIC

General Atomic Company
P.O. Box 81608 San Diego, California 92138